ACS OMEGA

http://pubs.acs.org/journal/acsodf

Article

Barium-Promoted Yttria−Zirconia-Supported Ni Catalyst for Hydrogen Production via the Dry Reforming of Methane: Role of Barium in the Phase Stabilization of Cubic ZrO_2

Ahmed Sadeq Al-Fatesh,* Rutu Patel, Vijay Kumar Srivastava, Ahmed Aidid Ibrahim, Muhammad Awais Naeem, Anis Hamza Fakeeha, Ahmed Elhag Abasaeed, Abdullah Ali Alquraini, and Rawesh Kumar*

Cite This: *ACS Omega* 2022, 7, 16468−16483

Read Online

ACCESS | Metrics & More | Article Recommendations | Supporting Information

ABSTRACT: Developing cost-effective nonprecious active metal-based catalysts for syngas (H_2/CO) production via the dry reforming of methane (DRM) for industrial applications has remained a challenge. Herein, we utilized a facile and scalable mechanochemical method to develop Ba-promoted (1−5 wt %) zirconia and yttria−zirconia-supported Ni-based DRM catalysts. BET surface area and porosity measurements, infrared, ultraviolet−visible, and Raman spectroscopy, transmission electron microscopy, and temperature-programmed cyclic (reduction−oxidation−reduction) experiments were performed to characterize and elucidate the catalytic performance of the synthesized materials. Among different catalysts tested, the inferior catalytic performance of 5Ni/Zr was attributed to the unstable monoclinic ZrO_2 support and weakly interacting NiO species whereas the 5Ni/YZr system performed better because of the stable cubic ZrO_2 phase and stronger metal−support interaction. It is established that the addition of Ba to the catalysts improves the oxygen-endowing capacity and stabilization of the cubic ZrO_2 and $BaZrO_3$ phases. Among the Ba-promoted catalysts, owing to the optimal active metal particle size and excess ionic CO_3^{2-} species, the 5Ni4Ba/YZr catalyst demonstrated a high, stable H_2 yield (i.e., 79% with a 0.94 H_2/CO ratio) for up to 7 h of time on stream. The 5Ni4Ba/YZr catalyst had the highest H_2 formation rate, 1.14 mol g^{-1} h^{-1} and lowest apparent activation energy, 20.07 kJ/mol, among all zirconia-supported Ni catalyst systems.

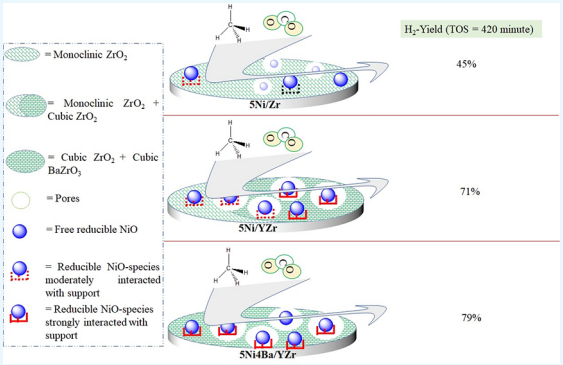

1. INTRODUCTION

The Paris Agreement set a goal for this century of keeping global warming below 2 °C and preferably at 1.5 °C. Aside from reducing anthropogenic greenhouse gas emissions (e.g., CO_2 and CH_4), turning these gases into value-added chemical feedstock is a more enticing way to accomplish this aim. In this context, the dry reforming of methane (DRM) is a potential and viable option because it yields hydrogen from the conversion of two major greenhouse gases (i.e., CH_4 and CO_2). Catalysts based on noble metals have been reported to be effective for DRM.[1−5] The total methane dissociation energy among the transition metals was found to follow the order Ni < Pd = Pt, so the experimental order of methane conversion was observed to be Ni > Pd = Pt.[6] Among Ni and Co, Gallego et al. found that the electronic configuration of Ni in Ni−CH_4 is $s^{0.54}d^{9.42}$ (with respect to the d^8s^2 electronic configuration of metallic Ni), indicating smaller steric repulsion between a closed shell of Ni and CH_4.[7] However, the electronic configuration of Co remains the same (either in Co−CH_4 or in metallic Co), causing a large repulsion between a closed shell of Co and CH_4. Importantly, the interaction energy of CH_4 with Ni is 18 kcal/mol, and with Co it is 0.7 kcal/mol. As a result, from a catalytic activity standpoint, Ni-based catalysts are more appealing for industrial applications than Co catalysts. However, high-temperature Ni sintering, which induces pronounced coke deposition and, eventually, catalyst deactivation, is a major challenge.

To stabilize the Ni, it has been dispersed on several metal oxides including Al_2O_3,[8] SiO_2,[9] zeolites,[10] ZrO_2,[11] TiO_2,[12] and MgO.[13] Furthermore, the addition of a promoter over supported Ni catalysts had brought about major physiochemical changes over the catalyst surface in favor of DRM. In brief, Mg incorporation added alkalinity to the catalyst system,[2,14−17]

Received: January 23, 2022
Accepted: April 20, 2022
Published: May 3, 2022

Sr boosted Lewis basicity,[18] Yb brought about a high edge of reducibilty,[19] Sc induced basicity and a metal−support interaction,[20] W stabilized the NiO phase and modified the redox behavior,[8,21,22] Ce or Y advanced lattice ion mobility together with reducibility,[23−39] and B or La induced carbon gasification (through B−OH species and $La_2O_2CO_3$ formation, respectively).[40−46] Likewise, the addition of Sm, Gd, or Mn−Al (equal proportions) optimized the Ni size and enhanced the metal−support interaction.[47−49] Among the various supports, ZrO_2 has the advantage of being able to withstand harsh thermal conditions while also supplying mobile oxygen species that can facilitate the oxidation of CH_4-derived coke deposits.[50,51] In the case of supported Ni/ZrO_2 catalysts, after reductive treatment, metallic Ni sites (i.e., Ni^0) and oxygen vacancies are formed. The reaction scheme over the Ni-supported catalyst system is shown in Figure 1. Generally,

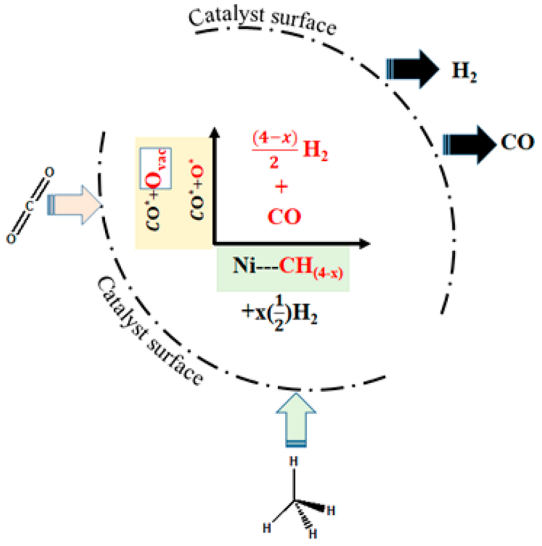

Figure 1. Reaction scheme over a Ni-supported catalyst system. O_{vac} is atomic oxygen that is formed after the dissociation of CO_2 at an oxygen vacancy. □ is an oxygen vacancy.

C−H cleavage occurs at Ni^0 sites, whereas CO_2 dissociation occurs preferably at oxygen vacancies. Because Ni has a strong interaction with CH_4,[7] CH_4 is decomposed over Ni^0 into $CH_{(4-x)}$ and $x(1/2)H_2$ (where x = 1, 2, 3, 4). CO_2, on the other hand, is adsorbed over basic surface sites and dissociates into CO and atomic oxygen/adsorbed oxygen at the Ni-support interface/boundary as well as on oxygen vacancies. Subsequently, the adsorbed oxygen oxidizes the formed $CH_{(4-x)}$ species into CO and $(4-x)(1/2)H_2$.[52] At the same time, the carbon deposit is oxidized by lattice oxygen from the support, leaving an oxygen vacancy behind. Following that, the oxygen vacancy is replenished by CO_2. This emphasizes the significance of adsorbed oxygen, which is directly involved in the oxidation of $CH_{(4-x)}$ species.

According to the literature, the conventionally synthesized Ni-impregnated ZrO_2 catalyst exhibited good DRM activity initially. However, because of a lack of optimal metal−support interactions, it underwent a high degree of graphitization and continuous catalyst deactivation.[53,54] On the other hand, sol−gel-derived catalysts demonstrated a strong metal−support interaction feature but required a costly synthetic procedure and produced fewer exposed active metal sites. However, by applying high Ni loading (10 wt %) and high-volume expansive carrier gas argon (8 times the feed gas volume), good catalytic activity was noticed.[55]

The ultimate challenges needed for a DRM reaction are the inhibition of carbon deposition on the catalyst surface and active metal sintering. Numerous approaches have been used by researchers to improve stability and to circumvent coke formation over Ni-based catalysts. It has been proposed that basicity improves the catalyst's ability to adsorb CO_2, facilitating coke gasification via the reverse Boudouard reaction (i.e., $2CO \leftrightarrow C + CO_2$). The addition of alkali or alkaline earth metals as promoters can improve the basic properties of the catalysts. These promoters may also enhance other features such as active metal dispersion and the metal−support interaction. For instance, 0.6% Na addition to a ZrO_2-supported Ni catalyst was found to increase the metal−support interaction by the formation of NiO_xH_y species and to inhibit the hydrogenation of carbon deposits.[55] Similarly, adding Ca to a Ni/ZrO_2 catalyst improves its basicity and textural properties, which in turn helps to avoid carbon deposition.[53,54] In the $^{13}CH_4$ isotope experiment, it was found that the ratio of "^{13}CO derived from CH_4" and "CO derived from CO_2" is 5/10 over a lanthana-zirconia-supported Ni catalyst, however, when Ca was used as a promoter, this ratio increased to 8/10.[56] That means that without Ca the majority of the CO was derived from CO_2, but upon Ca promotion, more interaction of CO_2 with the carbon impurity has taken place and more CO is generated by CH_4.

Among other basic promoters, barium (Ba) has previously been used to improve the thermal and catalytic properties of Ni-based materials. For instance, when Ni was deposited by chemical vapor deposition over the BaO-ZrO_2 support, it demonstrated the self-decoking ability of a carbon deposit by −OH and −O species with a negligible sign of Ni sintering for up to 50 h TOS at 700 °C.[57] Similarly, when barium is added to alumina, barium hexa-aluminate is formed, which has excellent thermal stability.[58,59] You et al. demonstrated that the addition of Ba to γ-Al_2O_3 can significantly neutralize the acidity of alumina.[60] Gomes et al. found that by substituting La with Ba in $LaNiO_3$ perovskite, resistance against deactivation had been improved.[61] BaO (4 wt %) addition over SiO_2-supported Ni enhanced the CO_2 methanation activity.[62] The BaO/Ni interface is known for the water-mediated oxidation of carbon deposits to CO.[63] Ersolmaz demonstrated that $BaCO_3$ is effective at oxidizing carbon through the formation of complexes between $BaCO_3$ and C, which can be decomposed to CO_2 at higher temperatures.[64] A barium zirconate-supported Ni catalyst has been utilized for a dry reforming reaction by Seo et al.[57] When BaO is combined with the ZrO_2−Y_2O_3 support, it forms the $BaZr_{0.9}Y_{0.1}O_{3-\delta}$ mixed oxide, which has a higher basicity than ZrO_2−Y_2O_3.[65] $BaZr_{0.9}Y_{0.1}O_{3-\delta}$ also exhibits a high proton conductivity, which may accelerate H-abstraction from the methyl group on the surface.[66] Promotional loading of $BaCO_3$ over the ZrO_2−Y_2O_3-supported Ni catalyst was well utilized in solid-oxide fuel cells for the direct utilization of methane[67] and the electrolysis of H_2O to H_2 and CO_2 to CO.[68] On the basis of these findings, we anticipate that BaO-promoted ZrO_2−Y_2O_3-supported Ni materials will have well-dispersed catalytically active sites (Ni^0), improved basic properties, high proton conductivity, and coke resistance in favor of DRM.

Among the various synthesis methods, mechanochemical synthesis has received a considerable amount of attention because of its simplicity and use of cheap precursors as well as

https://doi.org/10.1021/acsomega.2c00471
ACS Omega 2022, 7, 16468−16483

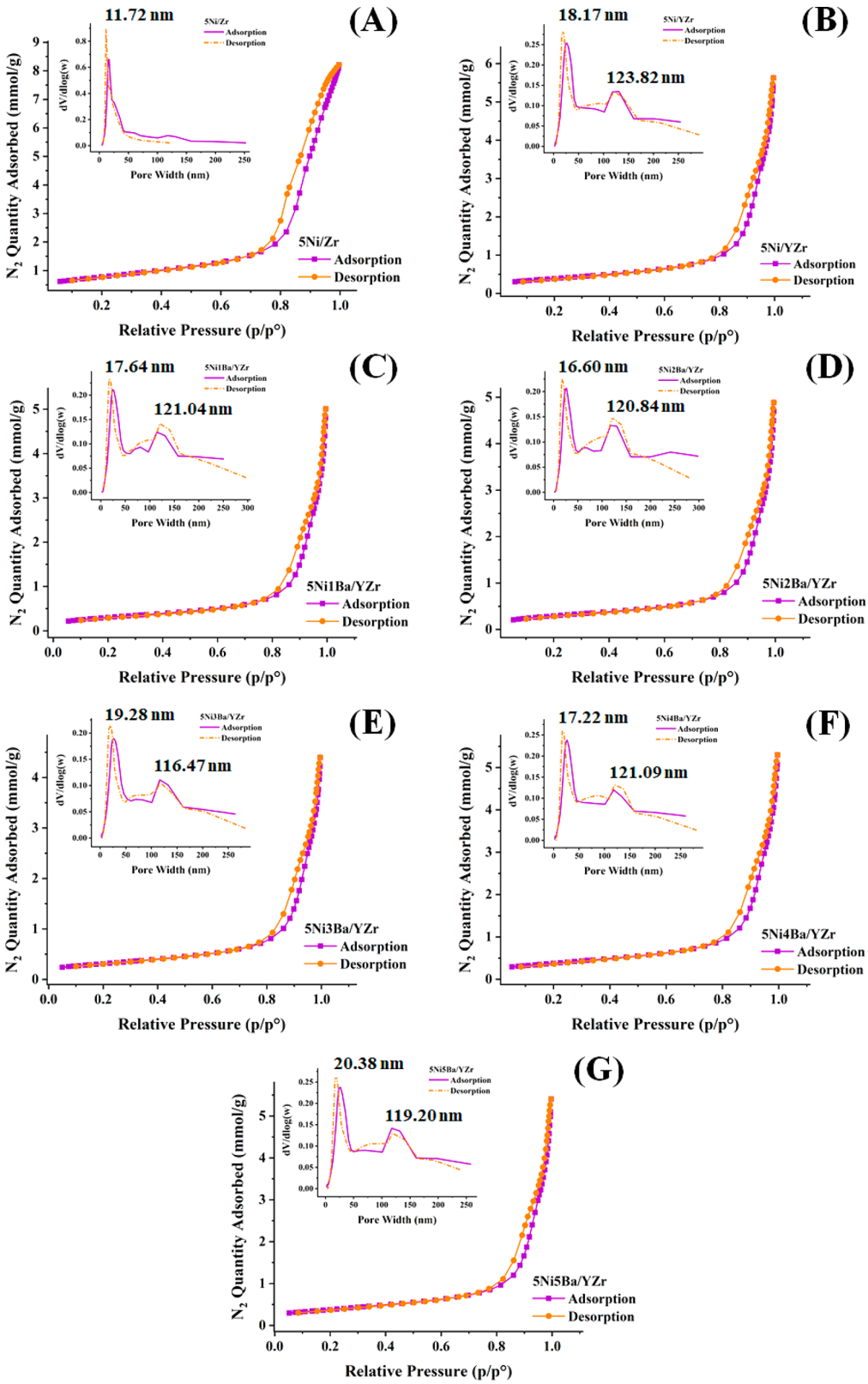

Figure 2. N_2 adsorption isotherm and porosity distribution profiles of (A) 5Ni/Zr, (B) 5Ni/YZr, (C) 5Ni1Ba/YZr, (D) 5Ni2Ba/YZr, (E) 5Ni3Ba/YZr, (F) 5Ni4Ba/YZr, and (G) 5Ni5Ba/YZr.

the possibility of realizing phases with different properties. Herein, we have systematically developed Ba-promoted (1−5 wt %) yttria−zirconia-supported Ni-based catalysts (5Ni*x*Ba/YZr; *x* = 1−5 wt %). These materials were tested for DRM and characterized by surface area porosity measurements, infrared, ultraviolet−visible and Raman spectroscopy, and transmission electron microscopy. We demonstrated that adding a Ba promoter to the Ni/YZr catalyst inhibits carbon formation.

https://doi.org/10.1021/acsomega.2c00471
ACS Omega 2022, 7, 16468−16483

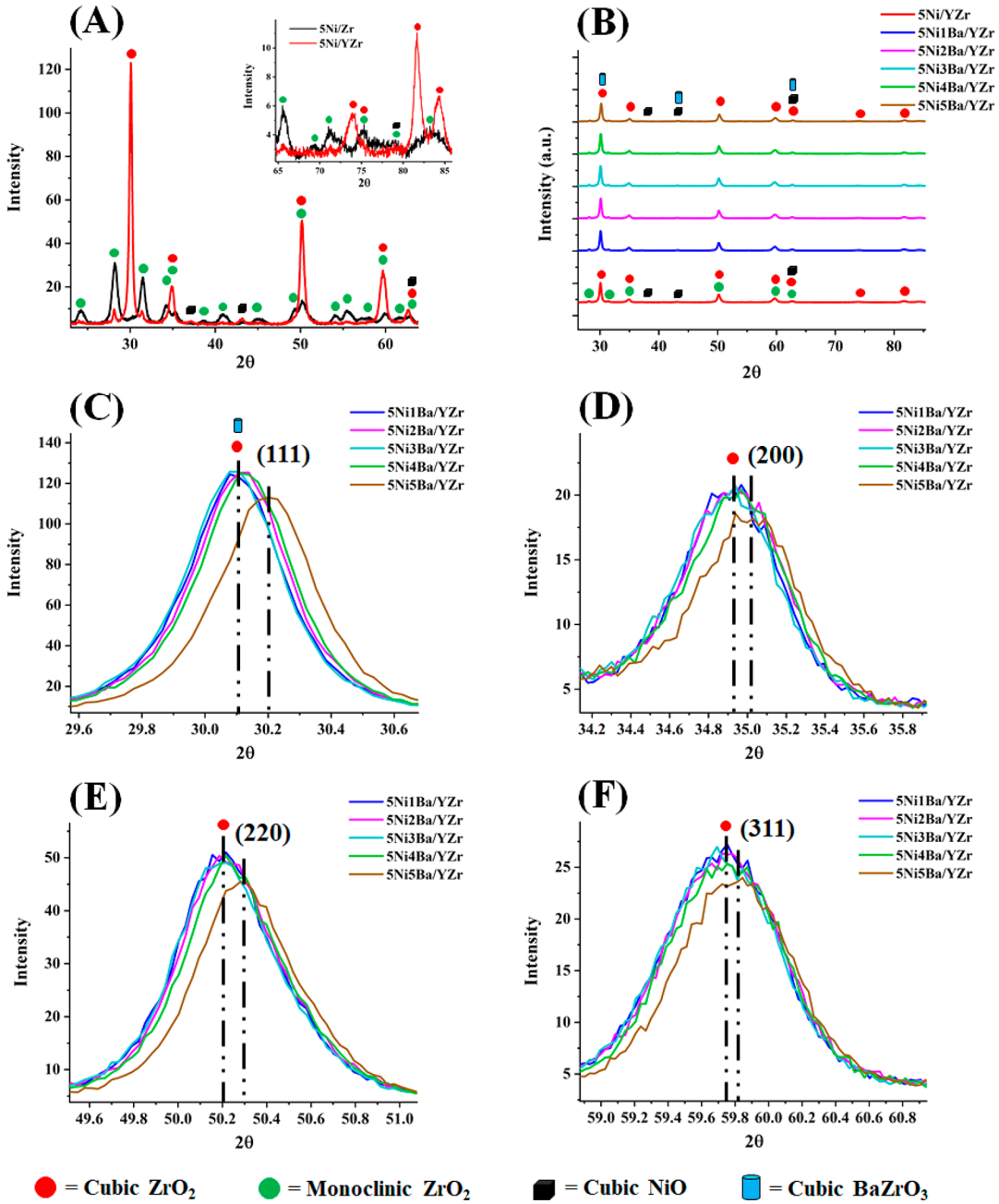

Figure 3. X-ray diffraction (XRD) profile of different catalyst samples (A) 5Ni/Zr and 5Ni/YZr. (B) Comparative XRD profiles of 5Ni*x*Ba/YZr (*x* = 0, 1, 2, 3, 4, and 5 wt %). (C−F) Peak shifts of the 5Ni5Ba/YZr catalyst around the (111), (200), (220), and (311) planes, respectively, as compared to other barium-promoted catalysts.

During the DRM reaction, catalyst surfaces are exposed to reducing gas (H_2) as well as oxidizing gas (CO_2). The reduction−oxidation−reduction cycles over catalyst surfaces are regulated during the entire DRM reaction. To establish the function−activity correlations, we performed cyclic H_2TPR-CO_2TPR-H_2TPR experiments in this study. These findings will contribute to advancing the knowledge spectrum of surface science toward DRM.

2. EXPERIMENT

2.1. Materials. Nickel nitrate hexahydrate (98%, Alfa Aesar), zirconia (gifted by Kagaku Daiichi Kogyo Co. Ltd Osaka), yttria (obtained from China), and deionized water were used.

2.2. Catalyst Preparation. The catalysts were prepared by the mechanochemical mixing of $Ni(NO_3)_2{\cdot}6H_2O$ (equivalent to 5 wt % Ni loading), $Ba(NO_3)_2$ (equivalent to 0, 1, 2, 3, 4, 5 wt % BaO loadings), and a mesoporous yttria-stabilized zirconia (8 wt % yttria, 92 wt % zirconia) support, followed by drying and calcination at 600 °C for 3 h. For convenience, the prepared catalysts are abbreviated as 5Ni*x*Ba/YZr, where Ni loading is fixed at 5 wt % and the Ba loading "*x*" varies from 0 to 5 wt % (i.e., *x* = 0, 1, 2, 3, 4, 5).

2.3. Catalyst Characterization. The catalysts that were synthesized were characterized using the Brunauer−Emmett−Teller (BET) surface area, X-ray diffraction (XRD), Raman spectroscopy, Fourier transform infrared spectroscopy (FTIR), ultraviolet−visible spectroscopy (UV−vis), transmission elec-

https://doi.org/10.1021/acsomega.2c00471
ACS Omega 2022, 7, 16468−16483

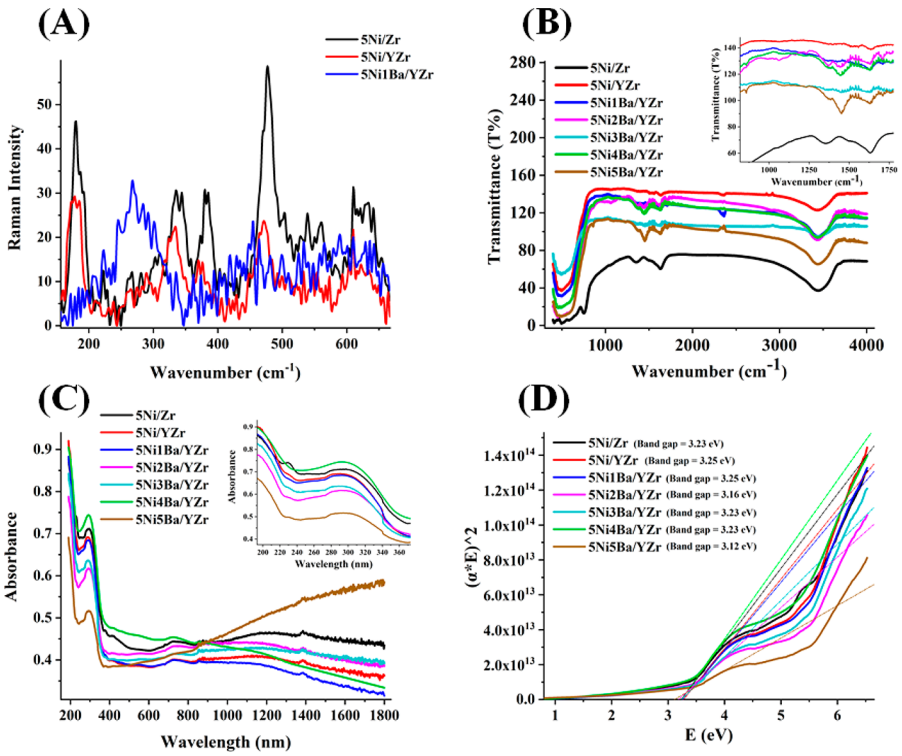

Figure 4. (A) Raman spectra. (B) IR spectra. (C) UV−vis spectra. (D) Band gaps of different catalyst samples.

tron microscopy (TEM), H_2 temperature-programmed reduction (H_2-TPR), CO_2 temperature-programmed desorption (CO_2-TPD) and thermogravimetric analysis (TGA). Detailed descriptions of the instruments and characterization procedures are provided in Supporting Information S1.

2.4. Catalyst Activity Test. The DRM experiments were carried out in a tubular stainless-steel reactor at a space velocity of 42 000 mL/h g_{cat} by passing a 30:30:10 mL/min volume ratio of a $CH_4/CO_2/N_2$ gas feed through 0.1 g of prereduced catalyst. All of the catalysts were prereduced under H_2 flow for 1 h at a flow rate of 30 mL/min at 600 °C. The DRM reaction was performed at 1 atm and 800 °C. The effluent was examined with an online GC equipped with molecular sieves 5A, Porapak Q columns, and a TCD detector using Ar carrier gas. The H_2 yield % was estimated with the following expression:

$$H_2\ \text{yield}\% = \frac{\text{moles of } H_2 \text{ produced}}{2 \times \text{moles of } CH_{4in}} \times 100$$

3. RESULTS

3.1. Characterization Results. A N_2 adsorption isotherm and the porosity distribution, BET surface area, pore volume, and pore diameter results of 5Ni/Zr and 5Ni*x*Ba/YZr (x = 0−5) catalysts are depicted in Figure 2, Figure S1, and Table S1. All materials have typical type IV isotherms with an H1 hysteresis loop indicating the presence of cylindrical mesopores. The dV/d log W vs W plot (where V is volume and W is the pore width) shows a rapid view of micropore, mesopore, and macropore distributions over the catalyst surface. The obtained results show that our catalysts have a bimodal pore size distribution. The marked change appeared in the lower pore width range of 10−50 nm and the intermediate pore width range of 100−150 nm, where the intensity of the earlier one was higher than that of the later.[69] The average pore size over Ni/YZr catalyst is 17.88 nm (Table S1). Interestingly, when yttria is incorporated, the pore size of the respective catalyst is increased to 24.78 nm. It is worth noting that the yttria−zirconia-supported Ni catalyst system has ∼50% less surface area but an ∼40% larger average pore size than the zirconia-supported Ni catalyst. However, no substantial structural changes in terms of pore volume and pore width are observed upon the incorporation of Ba into the Ni/YZr catalyst. In a Ba-promoted catalyst system, the pore size was typically in the 24−27 nm range (Table S1).

The X-ray diffraction pattern of different catalyst samples and the NiO and $BaZrO_3$ crystallite sizes are shown in Figure 3 and Table S2. The zirconia-supported Ni catalyst (Ni/Zr) has a monoclinic zirconia phase (at 2θ = 23.93, 28.18, 31.48, 34.78, 38.58, 40.85, 44.70, 49.37, 50.16, 54.04, 55.34, 58.14, 59.98, 61.68, 62.92, 65.60, 69.13, 71.20, 75.39, 78.97, and 83.56°; JCPDS reference no. 00-007-0343) and a cubic NiO phase (at 2θ = 37.12, 43.24, 62.92, 75.39, and 78.97°; JCPDS reference no. 00-004-0835). The presence of the monoclinic ZrO_2 phase in the 5Ni/Zr catalyst is also verified by Raman spectra (Figure 4A). The Raman bands related to the monoclinic ZrO_2 phase appeared at 179, 335, 379, 476, and 610 cm^{-1}.[70,71] Interestingly, over the yttria−zirconia-supported Ni catalyst were found more intense peaks of the cubic ZrO_2 phase (2θ = 30.08, 34.97, 50.10, 59.64, 62.59, 74.07, 75.39, 81.67, and 84.31°; JCPDS reference no. 00-003-0640) than of monoclinic ZrO_2. This indicates that yttria stabilizes the cubic phase of ZrO_2. The crystallite size of cubic NiO is increased to 38.8 nm in 5Ni/YZr (against 18.4 nm in the 5Ni/Zr catalyst) (Table S2). The 1 wt % barium-promoted yttria−zirconia-supported Ni catalyst mainly contains the cubic ZrO_2 phase. However, cubic $BaZrO_3$ Bragg reflections at 2θ = 30.10, 43.26, and 62.67° (JCPDS reference no. 00-006-0399) were also evident in this catalyst (Figure 3B). The presence of Ba−O in the

https://doi.org/10.1021/acsomega.2c00471
ACS Omega 2022, 7, 16468−16483

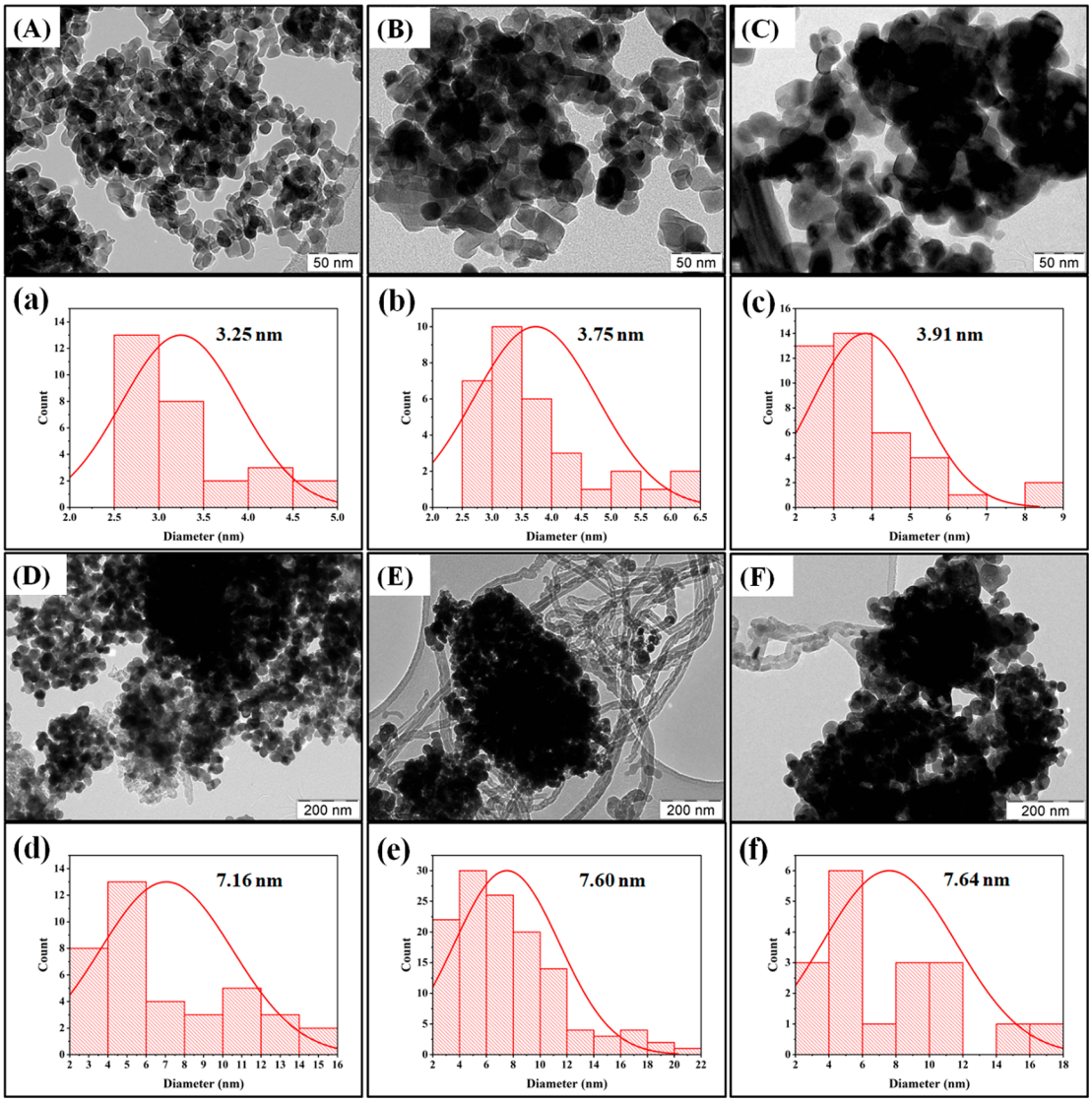

Figure 5. TEM micrographs and Ni particle size distributions of different catalyst samples. (A and a) Fresh 5Ni/Zr, (B and b) fresh 5Ni/YZr, (C and c) fresh 5Ni4Ba/YZr, (D and d) spent 5Ni/Zr, (E and e) spent 5Ni/YZr, and (F and f) spent 5Ni4Ba/YZr.

structure is also verified by the Raman spectra of the 5Ni1Ba/YZr catalyst. The Raman band at around 220−280 cm^{-1} over 5Ni1Ba/YZr is due to the overtones of TA, TA + TO, and TO of Ba−O vibrational modes[72] (Figure 4A). It can be said that Ba incorporation stabilizes the cubic phase of ZrO_2 pronouncedly. On increasing the Ba loading up to 4 wt %, the minimum sizes of NiO (18.7 nm) and $BaZrO_3$ (28.4 nm) crystallites were found. At 5 wt % Ba loading, selected planes (111, 200, 220, and 311) of cubic ZrO_2 peaks are shifted to a higher Bragg's angle, indicating a decrease in interplanar spacing (Figure 3C−F).

IR spectra, UV−vis spectra, and corresponding band-gap energy profiles of 5Ni/Zr and 5Ni*x*Ba/YZr (x = 0, 1, 2, 3, 4, and 5 wt %) catalyst systems are shown in Figure 4B−D, respectively. IR peaks due to the bending and stretching vibration of O−H are present at 1630 and 3444 cm^{-1}, respectively, in all catalysts.[22,73] The zirconia-supported Ni catalyst has vibrational peaks of Zr−O at 497 and 750 cm^{-1},[22] a broad peak of the bidentate format at 1355 cm^{-1},[74] and a unidentate carbonate peak at 1380 cm^{-1}.[37,73] Interestingly, in the yttria−zirconia-supported Ni catalyst, the vibrational peaks of Zr−O and bidentate format peaks disappeared, indicating that the addition of yttria brought about major changes in the bonding pattern. At higher Ba loadings (4 to 5 wt %), the stretching vibrations of CO_3^{-2} are observed at 851 and 1460 cm^{-1}.[75] However, at 2 wt % Ba, the symmetric stretching vibrational peak of CO_3^{-2} (C_{2v} or C_s symmetry) at 1084 cm^{-1}[76] and the stretching vibration of C═O at 1712 cm^{-1} are also noticed.[77]

The zirconia-supported Ni catalyst had O^{2-} (2p, valence band) to M^{n+} (4d, conduction band) charge-transition bands at 229 and 290 nm in the UV−vis spectra.[22] In comparing the UV spectra of Ni/Zr to those of ZrO_2, it is found that the peak intensity at 229 nm remains the same but the peak intensity at about 290 nm is increased as well as broadened upon Ni anchoring over ZrO_2. (Figure S2). This indicates that the peak at 229 nm is due to the charge-transfer band from O^{2-} to Zr^{4+} and that the peak at 290 is due to the charge-transfer band from O^{2-} to Ni^{2+} as well as that from O^{2-} to Zr^{4+}. On the other hand, for the yttria−zirconia-supported catalyst, the peak at 229 nm disappears, which indicates that yttria incorporation into the support changes the coordination environment of Zr^{4+}

https://doi.org/10.1021/acsomega.2c00471
ACS Omega 2022, 7, 16468−16483

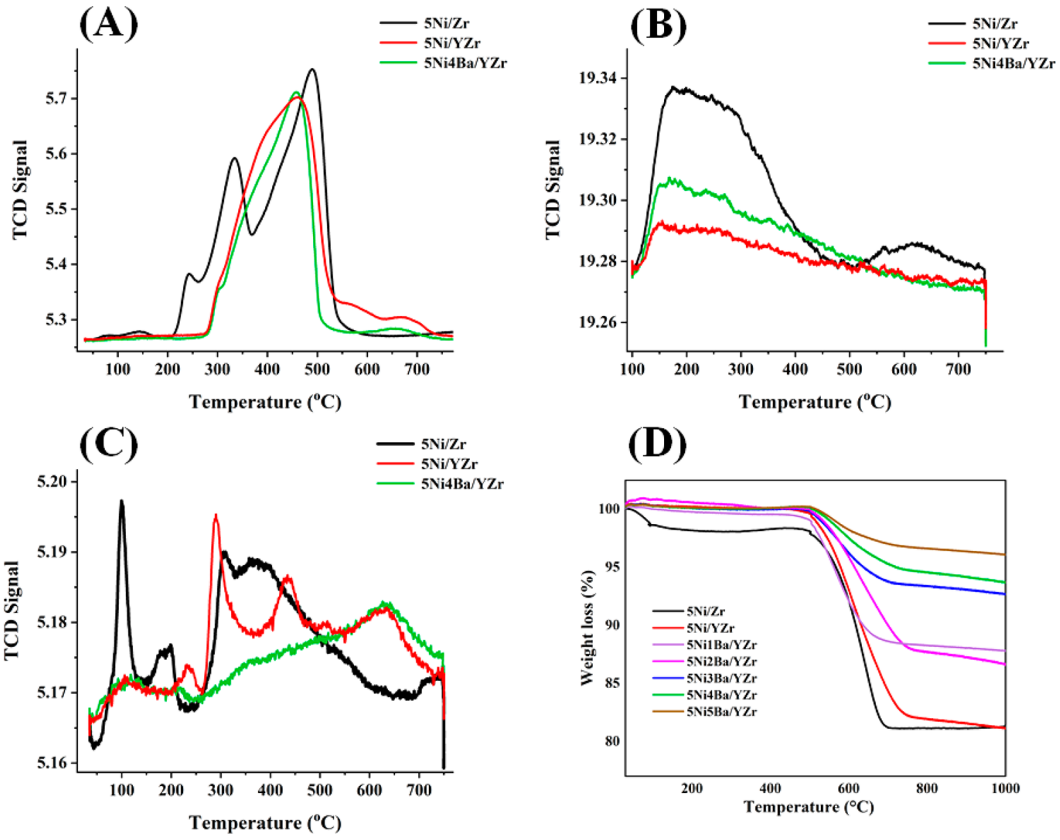

Figure 6. (A) H_2-TPR profile of 5Ni/Zr, 5Ni/YZr, and 5Ni4Ba/YZr. (B) CO_2TPD profile after H_2-TPR of 5Ni/Zr, 5Ni/YZr, and 5Ni4Ba/YZr. (C) H_2TPR-CO_2TPD-H_2TPR cycle of 5Ni/Zr, 5Ni/YZr, and 5Ni4Ba/YZr. (D) TGA profile of different catalyst samples.

exclusively. For most of these catalysts, the d−d transition bands at 378 and 418 nm for the d−d transition from the $^3A_{2g}(F)$ energy state to the $^3T_{1g}(P)$ energy state of Ni^{2+} (in the octahedral environment) and at 718 nm for the d−d transition from the $^3A_{2g}(F)$ energy state to the $^3T_{1g}(F)$ energy state of Ni^{2+} (in an octahedral environment) are found.[73] Indeed, these findings confirm the octahedral environment of Ni^{2+} in the 5Ni*x*Ba/YZr (x = 0−5 wt %) catalyst system. Interestingly, at a 4 wt % Ba loading, the charge transition from the O^{2-} (2p, valence band) to the Zr^{4+}/Ni^{2+} peak has the highest intensity but the d−d transition band for the $^3A_{2g}(F)$ energy state to the $^3T_{1g}(P)$ energy state of the Ni^{2+} octahedral environment disappeared. However, in this catalyst, the band gap was not affected by the addition of the Ba promoter (Figure 4D).

Figure 5 depicts TEM images of fresh and spent catalysts as well as their particle size distributions. Mean NiO particle sizes of 3.25, 3.75, and 3.91 nm are observed for 5Ni/Zr, 5Ni/YZr, and 5Ni4Ba/YZr catalysts, respectively. After the reaction, the particle sizes (Ni species) are grown to 7.16, 7.60, and 7.64 nm, respectively. For spent catalysts, the formation of carbon nanotubes is easily visible.

H_2-TPR, H_2-TPR followed by CO_2-TPD, and H_2TPR-CO_2TPD-H_2TPR cyclic profiles of different catalyst samples are shown in Figure 6 and Figure S3. The H_2-TPR profile of the zirconia-supported Ni catalyst (Ni/ZrO_2) shows a small reduction peak shoulder at about 235 °C for the reduction of free NiO, a sharp reduction peak at 335 °C for the reduction of NiO weakly interacting with the support, and a relatively smaller but broader peak at 490 °C for the reduction of NiO moderately interacting with the support (Figure 6A). When yttria was combined with the ZrO_2 support, the reduction peak for weakly interacting NiO species almost vanished, whereas the reduction peaks for NiO moderately interacting with the support remained. This indicates that the catalyst had a smaller quantity of reducible, weakly interacting NiO species and that the addition of yttria resulted in a stronger metal−support interaction. Importantly, the reduction profile of Ba-promoted catalysts is identical to that of 5Ni/YZr. The CO_2-TPD experiments were performed in conjunction with H_2-TPR over reduced 5Ni/Zr, 5Ni/YZr, and 5Ni5Ba/YZr catalysts in order to estimate the basic sites in these materials (Figure 6B). During the H_2-TPR, the reducible metal oxides are reduced to the respective metals and the surface hydroxyls are converted to water. As a result, the reducible NiO and surface hydroxyl ions should be eliminated during H_2-TPR treatment for these catalysts. The reduced 5Ni/Zr catalyst had a significant concentration of weak basic sites (surface hydroxyls) at low temperatures, moderate-strength basic sites (surface oxide ions) at intermediate temperatures, and strong basic sites (thermally stable surface carbonates) at high temperatures. This indicates that the surface anion that is present on 5Ni/Zr may not be reducible but basic. The yttria−zirconia-supported Ni catalyst had a good quantity of moderately interacting reducible NiO species, and during H_2-TPR treatment, they must be reduced to metallic Ni (by removing oxygen). Thus, the CO_2 TPD profile of the reduced 5Ni/YZr catalyst showed the absence of moderate strength basic sites. It also indicates the greater oxygen-endowing capacity of the YZr-supported Ni catalyst than the ZrO_2-supported Ni catalyst. The 5Ni4Ba/YZr catalyst had a good quantity of reducible, moderately interacting NiO species. However, a substantial number of intermediate-strength basic sites are present over the reduced

https://doi.org/10.1021/acsomega.2c00471
ACS Omega 2022, 7, 16468−16483

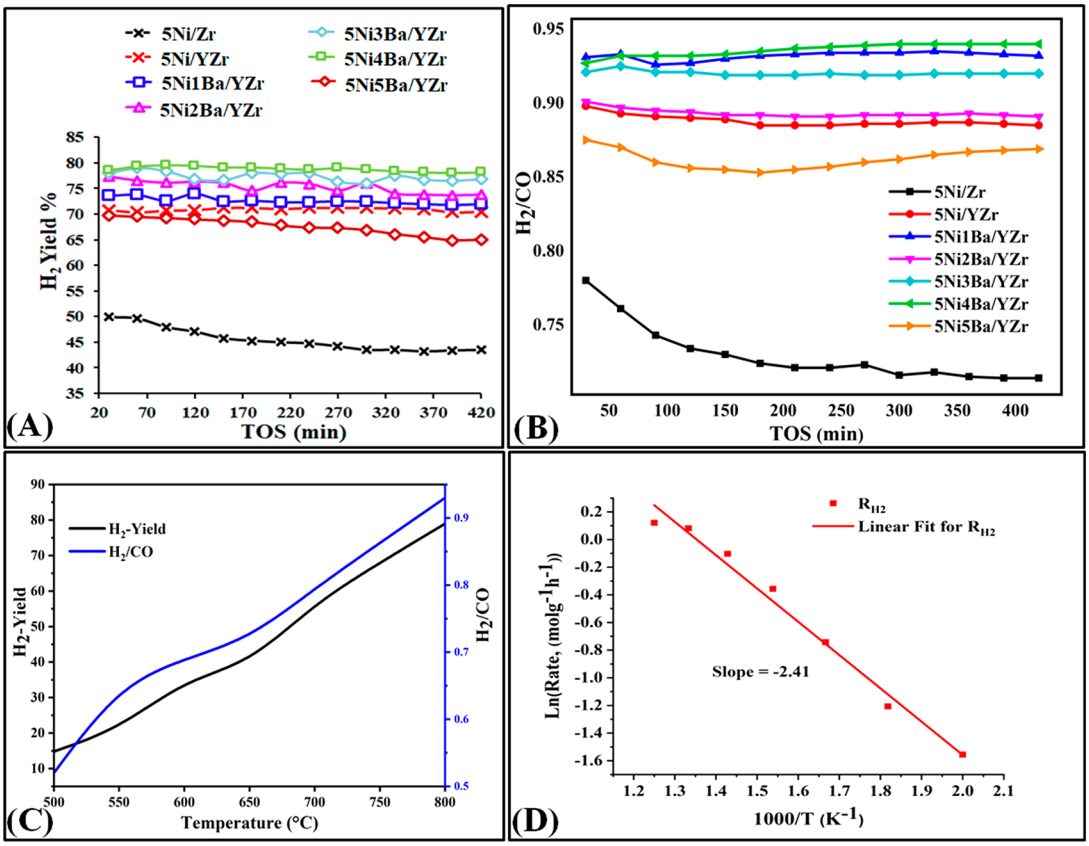

Figure 7. Catalytic activity results. (A) H_2 yield of different catalysts at 800 °C. (B) H_2/CO ratio of different catalysts at 800 °C. (C) H_2 yield and H_2/CO ratio of 5Ni4Ba/YZr at different reaction temperatures. (D) Influence of the reaction temperature on the H_2 formation rate of 5Ni4Ba/YZr.

5Ni4Ba/YZr catalyst. These results imply that the basic nature of BaO contributes to retaining the high surface basicity of the 5Ni4Ba/YZr catalyst.

H_2-TPR reduces NiO to metallic Ni while also creating oxygen vacancies in the underlying metal oxide support because of H_2 spillover from adjacent metallic Ni species. In general, such oxygen vacancies could be refilled when CO_2-TPD is combined with H_2-TPR. In this CO_2-TPD process, the reduced Ni is reoxidized to NiO. It is important to know the type of NiO that is regenerated following oxygen replenishment by CO_2. This can be achieved by performing another H_2-TPR over the H_2TPR-CO_2TPD treated catalyst (Figure 6C). The cyclic experiment (H_2TPR-CO_2TPD-H_2TPR) will provide evidence of the CO_2 replenishment capacity and the stability of Ni species across different catalyst systems. In the case of the zirconia-supported Ni catalyst, abundant reducible peaks for free NiO species and reducible moderately interacting NiO species are observed. Prominent reducible peaks for free NiO species indicate pronounced Ni sintering during the reduction−oxidation−reduction cycle, which may be the major cause of the inferior performance of the catalytic activity of the zirconia-supported Ni catalyst. In contrast, there is no free NiO reducible peak in the 5Ni/YZr catalyst, although there are peaks attributable to moderately and strongly interacting NiO species, which indicates that the yttria has improved the sintering resistance and strong metal−support interaction properties. Likewise, the broad reduction peak associated with strongly interacting NiO species is mainly observed in the case of the Ba-promoted catalyst.

The TGA profiles of the spent catalysts are shown in Figure 6D. The zirconia- and yttria−zirconia-supported Ni spent catalysts showed a significant weight loss due to the oxidation of surface carbon deposits. Notably, increasing the Ba loading reduces weight loss. It implies that the incorporation of Ba in the catalytic system decreases the extent of coke formation on the catalyst surface during the DRM reaction.

3.2. Catalytic Activity Results. The catalytic activity of 5Ni/YZr and 5Ni*x*Ba/YZr (x = 1−5 wt %) catalyst systems for DRM in terms of hydrogen yield is shown in Figure 7. The H_2 yield for a zirconia-supported catalyst (5Ni/Zr) is the lowest and is unstable with respect to the time on stream (TOS). It is 50% initially, which decreases to 45% within 420 min. In contrast, the yttria−zirconia-supported Ni catalyst (5Ni/YZr) has a higher stable H_2 yield for up to 420 min on TOS. It remains nearly stable at around 71% for 420 min. This suggests that incorporating yttria into the ZrO_2 support is beneficial to the catalyst system. Interestingly, when 1−5 wt % Bapromoter is added to a yttria−zirconia-supported Ni catalyst (5Ni*x*Ba/YZr; x = 1−5 wt %), prominent changes in the H_2 yield are observed. The H_2 yield remains more or less at about 72.5, 73, and 77% (for up to 420 min) over 1, 2, and 3 wt % BaO-promoted catalysts, respectively. The H_2 yield is highest (i.e., 78%) for a catalyst with 4 wt % Ba loading (5Ni4Ba/YZr), and it remains constant for up to 420 min on TOS. The 5Ni4Ba/YZr catalyst also maintains the highest H_2/CO ratio (i.e., 0.94) throughout the TOS (Figure 7B). The H_2/CO and H_2 yields increase as the reaction temperature increases from 500 to 800 °C, confirming the endothermic nature of the DRM reaction. Upon 5 wt % Ba, the H_2 yield drops sharply to 70% (even less

https://doi.org/10.1021/acsomega.2c00471
ACS Omega 2022, 7, 16468−16483

Table 1. Comparison of Apparent Activation Energies for H_2 Formation across Various Catalyst Systems

catalyst system	Ni wt %	reaction temp (°C)	R_{H_2}	slope	apparent activation energy (kJ/mol)	ref
5Ni4Ba/YZr	5	500	0.21	−2.41	20.07	our work
	5	550	0.30			
	5	600	0.48			
	5	650	0.70			
	5	700	0.90			
	5	750	1.08			
	5	800	1.13			
Ni/Zr	5	500	0.11	−3.27	27.19	43
	5	550	0.29			
	5	600	0.44			
	5	650	0.56			
	5	700	0.79			
Ni-CeO_2/ZrO_2	5	500	0.13	−3.08	25.61	43
	5	550	0.26			
	5	600	0.46			
	5	650	0.57			
	5	700	0.79			
Ni-La_2O_3/ZrO_2	5	500	0.22	−2.56	21.28	43
	5	550	0.35			
	5	600	0.54			
	5	650	0.69			
	5	700	0.98			
Ni-K_2O/ZrO_2	5	500	0.22	−2.62	21.78	43
	5	550	0.33			
	5	600	0.56			
	5	650	0.70			
	5	700	0.98			
Ni/ZrO_2-P	10	600	0.48	−1.57	13.05	133
	10	650	0.57			
	10	700	0.67			
	10	750	0.80			
	10	800	0.92			
Ni/ZrO_2-C	10	600	0.38	−2.16	17.96	133
	10	650	0.43			
	10	700	0.55			
	10	750	0.74			
	10	800	0.91			
5Ni/8PZr	5	600	0.05	−0.78	6.48	86
	5	650	0.71			
	5	700	0.07			
	5	750	0.10			
	5	800	0.18			
10Ni/8PZr	10	500	0.01	−4.28	35.58	86
	10	550	0.05			
	10	600	0.12			
	10	650	0.11			
	10	700	0.24			
	10	750	0.28			
	10	800	0.37			
15Ni/8PZr	15	500	0.07	−2.20	18.29	86
	15	550	0.13			
	15	600	0.14			
	15	650	0.25			
	15	700	0.29			
	15	750	0.32			
	15	800	0.40			
20Ni/8PZr	20	500	0.07	−2.23	18.54	86
	20	550	0.13			
	20	600	0.14			
	20	650	0.25			

https://doi.org/10.1021/acsomega.2c00471
ACS Omega 2022, 7, 16468−16483

Table 1. continued

catalyst system	Ni wt %	reaction temp (°C)	R_{H_2}	slope	apparent activation energy (kJ/mol)	ref
	20	700	0.29			
	20	750	0.32			
	20	800	0.42			
Ni-CaO-ZrO_2	13.76	600	5.85	−0.17	1.41	91
	13.76	650	5.87			
	13.76	700	5.81			
	13.76	750	5.48			
	13.76	800	5.25			
	13.76	850	5.28			
	13.76	900	5.44			
	13.76	950	5.34			
	13.76	1000	5.23			
	13.76	1050	5.23			
	13.76	1100	5.22			
	13.76	1150	5.13			
	13.76	1200	5.13			
Ni/Ce50-Zr50		550	0.01	−4.64	38.58	95
		600	0.01			
		650	0.03			
		700	0.05			
		750	0.08			
		800	0.11			
		850	0.13			
Ni-Mn/Ce50-Zr50		550	0.04	−1.67	13.88	95
		600	0.06			
		650	0.08			
		700	0.10			
		750	0.11			
		800	0.12			
		850	0.12			
Ni/MgO-ZrO_2	10	850	0.47	−4.46	37.08	88
	10	900	0.71			
	10	950	0.82			
	10	1000	1.06			
Ni-0.5K/MgO-ZrO_2	10	850	0.61	−3.49	29.01	88
	10	900	0.80			
	10	950	1.11			
	10	1000	1.08			
Ni-0.9K/MgO-ZrO_2	10	850	0.32	−4.02	33.42	88
	10	900	0.52			
	10	950	0.53			
	10	1000	0.71			
Ni-1.4K/MgO-ZrO_2	10	850	0.34	−3.44	28.60	88
	10	900	0.52			
	10	950	0.53			
	10	1000	0.65			
Ni-1.9K/MgO-ZrO_2	10	850	0.21	−6.12	50.88	88
	10	900	0.28			
	10	950	0.40			
	10	1000	0.61			

than for the 1 wt % Ba-promoted sample) and decreases further to 65% within 420 min on TOS. Excess BaO may cover the available catalytic active sites at a high Ba loading (5 wt %), resulting in inferior performance compared to that of its counterparts. It appears that 4 wt % Ba is the optimal promotor loading for the yttria−zirconia-supported Ni catalyst to obtain the maximal H_2 yield and high H_2/CO. The hydrogen-formation rate over the 5Ni4Ba/YZr catalyst was found to be 1.14 ($mol_{H_2}/g_{Cat}/h$). The effect of temperature on the H_2-formation rate was also investigated in the temperature range of 500−800 °C. The apparent activation energy of 20.07 kJ/K/mol was estimated for H_2 formation over the 5Ni4Ba/YZr catalyst.

4. DISCUSSION

The catalytic activity of the zirconia-supported Ni catalyst in DRM is due to Ni^{2+} in octahedral coordination, a large surface area, the pore volume, and the bidentate format/monodentate

https://doi.org/10.1021/acsomega.2c00471
ACS Omega 2022, 7, 16468−16483

carbonate species. However, the presence of a reducible free/weakly interacting NiO species, a small pore size, and unstable monoclinic ZrO_2 phases limits the activity. The H_2TPR-CO_2TPD-H_2TPR cyclic experiment displayed a prominent quantity of a reducible free NiO species/weakly interacted NiO species. Weak metal−support interaction leads to Ni sintering at high temperatures, which causes a prominent carbon deposit. The 5Ni/Zr catalyst exhibited only 45% H_2 yield on TOS, and the TGA results showed a huge weight loss due to coke removal from this catalyst.

On the other hand, the yttria−zirconia-supported Ni catalyst had a small surface area but a relatively larger pore size. Furthermore, it mainly featured a cubic ZrO_2 phase and reducible Ni^{2+} species that were in octahedral coordination and strongly interacted with the support. This strong metal−support interaction, together with cubic ZrO_2 phase stabilization, resulted in a 71% H_2 yield over the 5Ni/YZr catalyst. The H_2-TPR followed by the CO_2-TPD experiment showed that the 5Ni/YZr catalyst has a higher oxygen-endowing capacity than the Ni/Zr catalyst. Although the 5Ni/YZr catalyst experienced similar weight loss due to carbon removal as the 5Ni/Zr catalyst, it demonstrated stable catalytic performance (71% H_2 yield) for up to 420 min, which indicates that the type of carbon deposit is amorphous and oxidizable and so does not block the catalytic active sites.

Upon addition of Ba promoter, the cubic $BaZrO_3$ phase additionally stabilizes the cubic ZrO_2 phase. When the Ba loading increases, the TGA result shows less weight loss in the spent catalysts. This indicates a greater oxygen-endowing capacity of the catalyst upon increasing the Ba loading to oxidize carbon deposits during the DRM. Among all Ba-promoted samples, 5Ni4Ba/YZr possesses the smallest NiO crystals (18.7 nm), excess CO_3^{2-} ionic species, a high-intensity charge-transition band from O^{2-} (2p, valence band) to Zr^{4+}/Ni^{2+}, and an optimal metal−support interaction. H_2TPR followed by the CO_2 TPD experiment showed that the reduced 5Ni4Ba/YZr sample has a relatively more basic site concentration than the 5Ni/YZr catalyst. The H_2TPR-CO_2TPD-H_2TPR cyclic experiment shows the presence of only reducible NiO species strongly interacting with the support. It can be said that the metallic Ni species anchored on the cubic zirconia support facilitates CH_4 decomposition and that the resultant hydrocarbon intermediates are then oxidized by oxygen-containing surface species (e.g., ionic CO_3^{2-}) or lattice oxygen. It conveys the highest H_2 yield of 78% constantly up to 420 min on TOS. The 4 wt % Ba is the optimum loading for the highest H_2 yield. When the Ba loading is increased to 5 wt %, the lattice planes are compacted and the NiO crystallite size increases. The excess Ba covers the accessible catalytic active sites, which in turn lowers the catalytic activity and stability. The 5Ni5Ba/YZr catalyst shows an inferior H_2 yield even below that of the 5Ni1Ba/YZr catalyst.

The catalytic activity of the above-discussed DRM catalysts and the other set of 54 DRM catalysts[78−132] in terms of the H_2 yield, H_2 formation rate, and CO formation is shown in Table S3. The calculation details for hydrogen and CO formation rates are described in Supporting Information S2. Among the different catalysts synthesized in this study, the 5Ni4Ba/YZr catalyst showed the highest hydrogen formation rate (1.14 mol g^{-1} h^{-1}). On the basis of the results in Table S3, it seems that the Ba promoter is a better choice than Ga,[94] Mn,[95] Al,[49] Al−Mn,[49] Pr,[44] Sm,[37] and Nd[44] promoters in terms of achieving a high hydrogen formation rate. At a ≤5 wt % Ni loading, a >0.9 H_2/CO ratio, and a ≤0.1 g catalyst weight, Sc-,[20] La-,[41] Gd-,[48] and Ce[109]-promoted ordered mesoporous silica-supported Ni catalyst systems demonstrated a higher rate of H_2 formation than our catalyst system. Nevertheless, the additional cost of structure-directing agents and complex catalyst preparation procedures may limit the industrialization potential of these materials. Following silica, some zirconia-based Ni catalysts were found to be more competent than our catalyst system in terms of H_2 production via DRM, such as the Cr-promoted lantana−zirconia-supported Ni catalyst[93] Ce-promoted lantana−zirconia[96] catalyst, and tungstate−zirconia[22]-supported Ni catalyst. They showed 1.18 $molg^{-1}h^{-1}$, 1.23 $molg^{-1}h^{-1}$, 1.14 $molg^{-1}h^{-1}$ H_2 formation rate, respectively. Furthermore, we compared the apparent activation energy for H_2 formation among closely related zirconia-supported Ni catalyst systems (Table 1). Among 5 wt % Ni-loaded catalysts, the apparent activation energies of the 5Ni4Ba/YZr catalyst (this work) and phosphate−zirconia-supported catalyst (5Ni/8PZr)[86] were 20.07 and 6.48 kJ/mol, respectively. However, in terms of activity, the 5Ni/8PZr catalyst had a much lower rate of hydrogen formation than our 5Ni4Ba/YZr catalyst.[86]

5. CONCLUSIONS

Yttria−zirconia-supported Ni-based catalysts and 1−5 wt % Ba-promoted yttria−zirconia-supported Ni-based catalysts are characterized and tested in the dry reforming of methane. The 5Ni/Zr catalyst shows low catalytic activity of a 45% H_2 yield due to an unstable monoclinic ZrO_2 support and the presence of free/weakly interacting reducible NiO species. The high activity (71%) of the 5Ni/YZr catalyst is correlated with larger exposed pores and a stronger metal−support interaction through the thermally stable cubic ZrO_2 phase and the presence of moderately interacting reducible NiO species. Upon increasing the barium loading, the oxygen capacity increases and the carbon deposition decreases. The addition of 4 wt % barium brings about the $BaZrO_3$ cubic phase, cubic ZrO_2 phase, optimum NiO crystallite size (18.7 nm), excess ionic CO_3^{2-} species, improved basicity, and high intensity of the charge-transfer band. Reduction−oxidation−reduction treatment showed only reducible, strongly interacting NiO species over the catalyst surface. A 79% H_2 yield and a 0.94 H_2/CO ratio are achieved for up to 420 min over the 5Ni4Ba/YZr catalyst. Among different zirconia-supported Ni catalysts, the 5Ni4Ba/YZr catalyst had the highest H_2 formation rate (1.14 mol g^{-1} h^{-1}) and the minimum apparent activation energy of hydrogen formation (20.07 kJ/mol). For 5 wt % Ba-promoted catalysts, the excess Ba covers the accessible Ni active sites and reduces the catalytic activity and stability.

■ ASSOCIATED CONTENT

Supporting Information

The Supporting Information is available free of charge at https://pubs.acs.org/doi/10.1021/acsomega.2c00471.

Catalyst characterization; pore size distribution of different catalyst samples; surface area, pore volume, and pore size of different catalyst samples; crystalline size of NiO and $BaZrO_3$ for different catalyst samples; UV−vis spectra of ZrO_2 and 5Ni/Zr catalysts; H_2-TPR profile of catalyst samples 5Ni/Zr and 5NixBa/YZr (x = 0, 1, 2, 3, 4, and 5 wt %); catalyst activity of different catalyst (reported across the literature as DRM catalysts)

https://doi.org/10.1021/acsomega.2c00471
ACS Omega 2022, 7, 16468−16483

in terms of the conversion of CH_4 and the conversion of CO_2; yield of H_2; H_2/CO ratio; rates of hydrogen formation and CO formation, expression for calculating the rates of H_2 formation and CO formation from CO_2 conversion and CH_4 conversion data; and chromatograms of DRM product analysis over the 5Ni/Zr catalyst at 800 °C, DRM product analysis over the 5Ni/YZr catalyst at 800 °C, and DRM product analysis over the 5Ni4Ba/YZr catalyst at 800 °C (PDF)

AUTHOR INFORMATION

Corresponding Authors

Ahmed Sadeq Al-Fatesh − *Chemical Engineering Department, College of Engineering, King Saud University, Riyadh 11421, Saudi Arabia;* orcid.org/0000-0002-5521-5741; Email: aalfatesh@ksu.edu.sa

Rawesh Kumar − *Department of Chemistry, Indus University, Ahmedabad, Gujarat, India 382115*; Email: kr.rawesh@gmail.com

Authors

Rutu Patel − *Department of Chemistry, Sankalchand Patel University, Visnagar, Gujarat, India 384315*

Vijay Kumar Srivastava − *Department of Chemistry, Indus University, Ahmedabad, Gujarat, India 382115*

Ahmed Aidid Ibrahim − *Chemical Engineering Department, College of Engineering, King Saud University, Riyadh 11421, Saudi Arabia*

Muhammad Awais Naeem − *ETH Zürich, Department of Mechanical and Process Engineering, CH 8092 Zürich, Switzerland*

Anis Hamza Fakeeha − *Chemical Engineering Department, College of Engineering, King Saud University, Riyadh 11421, Saudi Arabia*

Ahmed Elhag Abasaeed − *Chemical Engineering Department, College of Engineering, King Saud University, Riyadh 11421, Saudi Arabia*

Abdullah Ali Alquraini − *Chemical Engineering Department, College of Engineering, King Saud University, Riyadh 11421, Saudi Arabia*

Complete contact information is available at: https://pubs.acs.org/10.1021/acsomega.2c00471

Notes

The authors declare no competing financial interest.

ACKNOWLEDGMENTS

The authors extend their sincere appreciation to the Researchers Supporting Project (no. RSP-2021/368), King Saud University, Riyadh, Saudi Arabia. R.P. acknowledges the administration of Sankalchand Patel University and the SHODH Program for providing the research environment. R.K. and V.K.S. acknowledge Indus University.

REFERENCES

(1) Fakeeha, A. H.; Al Fatesh, A. S.; Ibrahim, A. A.; Kurdi, A. N.; Abasaeed, A. E. Yttria Modified ZrO_2 Supported Ni Catalysts for CO_2 Reforming of Methane: The Role of Ce Promoter. *ACS Omega* **2021**, *6* (2), 1280−1288.

(2) Al-Fatesh, A. S.; Kumar, R.; Fakeeha, A. H.; Kasim, S. O.; Khatri, J.; Ibrahim, A. A.; Arasheed, R.; Alabdulsalam, M.; Lanre, M. S.; Osman, A. I.; Abasaeed, A. E.; Bagabas, A. Promotional Effect of Magnesium Oxide for a Stable Nickel-Based Catalyst in Dry Reforming of Methane. *Sci. Rep.* **2020**, *10* (1), 13861.

(3) García-Diéguez, M.; Pieta, I. S.; Herrera, M. C.; Larrubia, M. A.; Alemany, L. J. Nanostructured Pt- and Ni-Based Catalysts for CO_2-Reforming of Methane. *J. Catal.* **2010**, *270* (1), 136−145.

(4) Anil, C.; Modak, J. M.; Madras, G. Syngas Production via CO_2 Reforming of Methane over Noble Metal (Ru, Pt, and Pd) Doped $LaAlO_3$ Perovskite Catalyst. *Mol. Catal.* **2020**, *484* (January), 110805.

(5) Yentekakis, I. V.; Goula, G.; Hatzisymeon, M.; Betsi-Argyropoulou, I.; Botzolaki, G.; Kousi, K.; Kondarides, D. I.; Taylor, M. J.; Parlett, C. M. A.; Osatiashtiani, A.; Kyriakou, G.; Holgado, J. P.; Lambert, R. M. Effect of Support Oxygen Storage Capacity on the Catalytic Performance of Rh Nanoparticles for CO_2 Reforming of Methane. *Appl. Catal. B Environ.* **2019**, *243*, 490−501.

(6) Liao, M.-S.; Au, C.-T.; Ng, C.-F. Methane Dissociation on Ni, Pd, Pt and Cu Metal (111) Surfaces - A Theoretical Comparative Study. *Chem. Phys. Lett.* **1997**, *272* (5−6), 445−452.

(7) Gallego, G. S.; Batiot-Dupeyrat, C.; Barrault, J.; Florez, E.; Mondragón, F. Dry Reforming of Methane over $LaNi_{1-Y}B_yO_{3\pm\delta}$ (B = Mg, Co) Perovskites Used as Catalyst Precursor. *Appl. Catal. A Gen.* **2008**, *334* (1−2), 251−258.

(8) Al-Fatesh, A. S.; Kumar, R.; Kasim, S. O.; Ibrahim, A. A.; Fakeeha, A. H.; Abasaeed, A. E.; Alrasheed, R.; Bagabas, A.; Chaudhary, M. L.; Frusteri, F.; Chowdhury, B. The Effect of Modifier Identity on the Performance of Ni-Based Catalyst Supported on γ-Al_2O_3 in Dry Reforming of Methane. *Catal. Today* **2020**, *348* (September), 236−242.

(9) Pantaleo, G.; Parola, V.; La; Testa, M. L.; Venezia, A. M. CO_2 Reforming of CH_4 over SiO_2-Supported Ni Catalyst: Effect of Sn as Support and Metal Promoter. *Ind. Eng. Chem. Res.* **2021**, *60* (51), 18684−18694.

(10) Najfach, A. J.; Almquist, C. B.; Edelmann, R. E. Effect of Manganese and Zeolite Composition on Zeolite-Supported Ni-Catalysts for Dry Reforming of Methane. *Catal. Today* **2021**, *369*, 31−47.

(11) Wang, Y.; Yao, L.; Wang, Y.; Wang, S.; Zhao, Q.; Mao, D.; Hu, C. Low-Temperature Catalytic CO_2 Dry Reforming of Methane on Ni-Si/ZrO_2 Catalyst. *ACS Catal.* **2018**, *8* (7), 6495−6506.

(12) Nguyen, H. M.; Pham, G. H.; Tade, M.; Phan, C.; Vagnoni, R.; Liu, S. Microwave-Assisted Dry and Bi-Reforming of Methane over M-Mo/TiO_2(M = Co, Cu) Bimetallic Catalysts. *Energy Fuels* **2020**, *34* (6), 7284−7294.

(13) Zuo, Z.; Liu, S.; Wang, Z.; Liu, C.; Huang, W.; Huang, J.; Liu, P. Dry Reforming of Methane on Single-Site Ni/MgO Catalysts: Importance of Site Confinement. *ACS Catal.* **2018**, *8* (10), 9821−9835.

(14) Taherian, Z.; Khataee, A.; Orooji, Y. Nickel-Based Nanocatalysts Promoted over MgO-Modified SBA-16 for Dry Reforming of Methane for Syngas Production: Impact of Support and Promoters. *J. Energy Inst.* **2021**, *97*, 100−108.

(15) Taherian, Z.; Khataee, A.; Orooji, Y. Facile Synthesis of Yttria-Promoted Nickel Catalysts Supported on MgO-MCM-41 for Syngas Production from Greenhouse Gases. *Renew. Sustain. Energy Rev.* **2020**, *134* (July), 110130.

(16) Alipour, Z.; Rezaei, M.; Meshkani, F. Effects of Support Modifiers on the Catalytic Performance of Ni/Al_2O_3 Catalyst in CO_2 Reforming of Methane. *Fuel* **2014**, *129*, 197−203.

(17) Titus, J.; Goepel, M.; Schunk, S. A.; Wilde, N.; Gläser, R. The Role of Acid/Base Properties in Ni/MgO-ZrO_2−Based Catalysts for Dry Reforming of Methane. *Catal. Commun.* **2017**, *100*, 76−80.

(18) Al-Fatesh, A. S.; Naeem, M. A.; Fakeeha, A. H.; Abasaeed, A. E. CO_2 Reforming of Methane to Produce Syngas over γ-Al_2O_3 -Supported Ni−Sr Catalysts. *Bull. Chem. Soc. Jpn.* **2013**, *86* (6), 742−748.

(19) Amin, M. H.; Mantri, K.; Newnham, J.; Tardio, J.; Bhargava, S. K. Highly Stable Ytterbium Promoted Ni /γ-Al_2O_3 Catalysts for Carbon Dioxide Reforming of Methane. *Applied Catal. B, Environ.* **2012**, *119*−*120*, 217−226.

https://doi.org/10.1021/acsomega.2c00471
ACS Omega 2022, 7, 16468−16483

(20) Al-Fatesh, A. S.; Atia, H.; Abu-Dahrieh, J. K.; Ibrahim, A. A.; Eckelt, R.; Armbruster, U.; Abasaeed, A. E.; Fakeeha, A. H. Hydrogen Production from CH_4 Dry Reforming over Sc Promoted Ni /MCM-41. *Int. J. Hydrogen Energy* **2019**, *44*, 20770−20781.
(21) Al-Fatesh, A. S.; Chaudhary, M. L.; Fakeeha, A. H.; Ibrahim, A. A.; Al-Mubaddel, F.; Kasim, S. O.; Albaqmaa, Y. A.; Bagabas, A. A.; Patel, R.; Kumar, R. Role of Mixed Oxides in Hydrogen Production through the Dry Reforming of Methane over Nickel Catalysts Supported on Modified γ-Al_2O_3. *Processes* **2021**, *9* (1), 157.
(22) Patel, R.; Al-Fatesh, A. S.; Fakeeha, A. H.; Arafat, Y.; Kasim, S. O.; Ibrahim, A. A.; Al-Zahrani, S. A.; Abasaeed, A. E.; Srivastava, V. K.; Kumar, R. Impact of Ceria over WO_3−ZrO_2 Supported Ni Catalyst towards Hydrogen Production through Dry Reforming of Methane. *Int. J. Hydrogen Energy* **2021**, *46*, 25015−25028.
(23) Goula, M. A.; Charisiou, N. D.; Siakavelas, G.; Tzounis, L.; Tsiaoussis, I.; Panagiotopoulou, P.; Goula, G.; Yentekakis, I. V. Syngas Production via the Biogas Dry Reforming Reaction over Ni Supported on Zirconia Modified with CeO2 or La_2O_3 Catalysts. *Int. J. Hydrogen Energy* **2017**, *42* (19), 13724−13740.
(24) Montoya, J. A.; Romero-Pascual, E.; Gimon, C.; Del Angel, P.; Monzón, A. Methane Reforming with CO_2 over Ni/ZrO_2-CeO_2 Catalysts Prepared by Sol-Gel. *Catal. Today* **2000**, *63* (1), 71−85.
(25) Laosiripojana, N.; Sutthisripok, W.; Assabumrungrat, S. Synthesis Gas Production from Dry Reforming of Methane over CeO_2 Doped Ni/Al_2O_3: Influence of the Doping Ceria on the Resistance toward Carbon Formation. *Chem. Eng. J.* **2005**, *112* (1−3), 13−22.
(26) Chein, R. Y.; Fung, W. Y. Syngas Production via Dry Reforming of Methane over CeO_2 Modified Ni/Al_2O_3 Catalysts. *Int. J. Hydrogen Energy* **2019**, *44* (28), 14303−14315.
(27) Wang, F.; Han, K.; Yu, W.; Zhao, L.; Wang, Y.; Wang, X.; Yu, H.; Shi, W. Low Temperature CO_2 Reforming with Methane Reaction over CeO_2-Modified Ni@SiO_2Catalysts. *ACS Appl. Mater. Interfaces* **2020**, *12* (31), 35022−35034.
(28) Han, K.; Yu, W.; Xu, L.; Deng, Z.; Yu, H.; Wang, F. Reducing Carbon Deposition and Enhancing Reaction Stability by Ceria for Methane Dry Reforming over Ni@SiO_2@CeO_2 Catalyst. *Fuel* **2021**, *291* (January), 120182.
(29) Han, K.; Wang, Y.; Wang, S.; Liu, Q.; Deng, Z.; Wang, F. Narrowing Band Gap Energy of CeO_2 in (Ni/CeO_2)@SiO_2 Catalyst for Photothermal Methane Dry Reforming. *Chem. Eng. J.* **2021**, *421* (April), 129989.
(30) Zhao, X.; Li, H.; Zhang, J.; Shi, L.; Zhang, D. Design and Synthesis of NiCe@m-SiO_2 Yolk-Shell Framework Catalysts with Improved Coke- and Sintering-Resistance in Dry Reforming of Methane. *Int. J. Hydrogen Energy* **2016**, *41* (4), 2447−2456.
(31) Albarazi, A.; Gálvez, M. E.; Da Costa, P. Synthesis Strategies of Ceria-Zirconia Doped Ni/SBA-15 Catalysts for Methane Dry Reforming. *Catal. Commun.* **2015**, *59*, 108−112.
(32) Setiabudi, H. D.; Chong, C. C.; Abed, S. M.; Teh, L. P.; Chin, S. Y. Comparative Study of Ni-Ce Loading Method: Beneficial Effect of Ultrasonic-Assisted Impregnation Method in CO_2 Reforming of CH_4 over Ni-Ce/SBA-15. *J. Environ. Chem. Eng.* **2018**, *6* (1), 745−753.
(33) Kumar, P.; Sun, Y.; Idem, R. O. Comparative Study of Ni-Based Mixed Oxide Catalyst for Carbon Dioxide Reforming of Methane. *Energy Fuels* **2008**, *22* (6), 3575−3582.
(34) Wolfbeisser, A.; Sophiphun, O.; Bernardi, J.; Wittayakun, J.; Föttinger, K.; Rupprechter, G. Methane Dry Reforming over Ceria-Zirconia Supported Ni Catalysts. *Catal. Today* **2016**, *277*, 234−245.
(35) Roh, H. S.; Potdar, H. S.; Jun, K. W. Carbon Dioxide Reforming of Methane over Co-Precipitated Ni-CeO_2, Ni-ZrO_2 and Ni-Ce-ZrO_2 Catalysts. *Catal. Today* **2004**, *93*−*95*, 39−44.
(36) Marinho, A. L. A.; Rabelo-Neto, R. C.; Epron, F.; Bion, N.; Toniolo, F. S.; Noronha, F. B. Embedded Ni Nanoparticles in $CeZrO_2$ as Stable Catalyst for Dry Reforming of Methane. *Appl. Catal. B Environ.* **2020**, *268*, 118387.
(37) Zhang, M.; Zhang, J.; Zhou, Z.; Chen, S.; Zhang, T.; Song, F.; Zhang, Q.; Tsubaki, N.; Tan, Y.; Han, Y. Effects of the Surface Adsorbed Oxygen Species Tuned by Rare-Earth Metal Doping on Dry Reforming of Methane over Ni/ZrO_2 Catalyst. *Appl. Catal. B Environ.* **2020**, *264*, 118522.
(38) Wang, Y.; Li, L.; Wang, Y.; Da Costa, P.; Hu, C. Highly Carbon-Resistant Y Doped NiO−ZrO_2 Catalysts for Dry Reforming of Methane. *Catalysts* **2019**, *9* (12), 1055.
(39) Bellido, J. D. A.; Assaf, E. M. Effect of the Y_2O_3-ZrO_2 Support Composition on Nickel Catalyst Evaluated in Dry Reforming of Methane. *Appl. Catal. A Gen.* **2009**, *352* (1−2), 179−187.
(40) Singh, S.; Nguyen, T. D.; Siang, T. J.; Phuong, P. T. T.; Huy Phuc, N. H.; Truong, Q. D.; Lam, S. S.; Vo, D. V. N. Boron-Doped Ni/SBA-15 Catalysts with Enhanced Coke Resistance and Catalytic Performance for Dry Reforming of Methane. *J. Energy Inst.* **2020**, *93* (1), 31−42.
(41) Oemar, U.; Kathiraser, Y.; Mo, L.; Ho, X. K.; Kawi, S. CO_2 Reforming of Methane over Highly Active La-Promoted Ni Supported on SBA-15 Catalysts: Mechanism and Kinetic Modelling. *Catal. Sci. Technol.* **2016**, *6* (4), 1173−1186.
(42) Lanre, M. S.; Al-Fatesh, A. S.; Fakeeha, A. H.; Kasim, S. O.; Ibrahim, A. A.; Al-Awadi, A. S.; Al-Zahrani, A. A.; Abasaeed, A. E. Catalytic Performance of Lanthanum Promoted Ni/ZrO_2 for Carbon Dioxide Reforming of Methane. *Processes* **2020**, *8* (11), 1502.
(43) Rezaei, M.; Alavi, S. M.; Sahebdelfar, S.; Bai, P.; Liu, X.; Yan, Z. F. CO_2 Reforming of CH_4 over Nanocrystalline Zirconia-Supported Nickel. *Catalysts. Appl. Catal. B Environ.* **2008**, *77* (3−4), 346−354.
(44) Yabe, T.; Mitarai, K.; Oshima, K.; Ogo, S.; Sekine, Y. Low-Temperature Dry Reforming of Methane to Produce Syngas in an Electric Field over La-Doped Ni/ZrO_2 catalysts. *Fuel Process. Technol.* **2017**, *158*, 96−103.
(45) Sokolov, S.; Kondratenko, E. V.; Pohl, M. M.; Rodemerck, U. Effect of Calcination Conditions on Time On-Stream Performance of Ni/La_2O_3-ZrO_2 in Low-Temperature Dry Reforming of Methane. *Int. J. Hydrogen Energy* **2013**, *38* (36), 16121−16132.
(46) Guo, Y. H.; Xia, C.; Liu, B. S. Catalytic Properties and Stability of Cubic Mesoporous $La_xNi_yO_z$/KIT-6 Catalysts for CO_2 Reforming of CH_4. *Chem. Eng. J.* **2014**, *237*, 421−429.
(47) Taherian, Z.; Yousefpour, M.; Tajally, M.; Khoshandam, B. Promotional Effect of Samarium on the Activity and Stability of Ni-SBA-15 Catalysts in Dry Reforming of Methane. *Microporous Mesoporous Mater.* **2017**, *251*, 9−18.
(48) Al-Fatesh, A. S.; Hanan atia; Ibrahim, A. A.; Fakeeha, A. H.; Singh, S. K.; Labhsetwar, N. K.; Shaikh, H.; Qasim, S. O. CO_2 Reforming of CH_4: Effect of Gd as Promoter for Ni Supported over MCM-41 as Catalyst. *Renew. Energy* **2019**, *140*, 658−667.
(49) Wang, Y.; Li, L.; Cui, C.; Da. Costa, P.; Hu, C. The Effect of Adsorbed Oxygen Species on Carbon-Resistance of Ni-Zr Catalyst Modified by Al and Mn for Dry Reforming of Methane. *Catal. Today* **2022**, *384*−*386* (March), 257−264.
(50) Zhang, X.; Wang, F.; Song, Z.; Zhang, S. Comparison of Carbon Deposition Features between Ni/ZrO_2 and Ni/SBA-15 for the Dry Reforming of Methane. *React. Kinet. Mech. Catal.* **2020**, *129* (1), 457−470.
(51) Zhang, Y.; Zhang, Y.; Zhao, Y.; Otroshchenko, T.; Perechodjuk, A.; Kondratenko, V. A.; Bartling, S.; Rodemerck, U.; Linke, D.; Jiao, H.; Jiang, G.; Kondratenko, E. V. Structure-Activity-Selectivity Relationships in Propane Dehydrogenation over Rh/ZrO_2Catalysts. *ACS Catal.* **2020**, *10* (11), 6377−6388.
(52) Barroso Quiroga, M. M.; Castro Luna, A. E. Kinetic Analysis of Rate Data for Dry Reforming of Methane. *Kinet. Catal. React. Eng.* **2007**, *46*, 5265−5270.
(53) Wang, C.; Sun, N.; Zhao, N.; Wei, W.; Zhang, J.; Zhao, T.; Sun, Y.; Sun, C.; Liu, H.; Snape, C. E. The Properties of Individual Carbon Residuals and Their Influence on the Deactivation of Ni-CaO-ZrO2 Catalysts in CH_4 Dry Reforming. *ChemCatChem.* **2014**, *6* (2), 640−648.
(54) Sun, N.; Wen, X.; Wang, F.; Peng, W.; Zhao, N.; Xiao, F.; Wei, W.; Sun, Y.; Kang, J. Catalytic Performance and Characterization of Ni-CaO-ZrO_2 Catalysts for Dry Reforming of Methane. *Appl. Surf. Sci.* **2011**, *257* (21), 9169−9176.

https://doi.org/10.1021/acsomega.2c00471
ACS Omega 2022, 7, 16468−16483

(55) Wang, Y.; Zhao, Q.; Wang, Y.; Hu, C.; Da Costa, P. One-Step Synthesis of Highly Active and Stable Ni-ZrO_x for Dry Reforming of Methane. *Ind. Eng. Chem. Res.* **2020**, *59* (25), 11441−11452.
(56) Bachiller-Baeza, B.; Mateos-Pedrero, C.; Soria, M. A.; Guerrero-Ruiz, A.; Rodemerck, U.; Rodríguez-Ramos, I. Transient Studies of Low-Temperature Dry Reforming of Methane over Ni-CaO/ZrO_2-La_2O_3. *Appl. Catal. B Environ.* **2013**, *129*, 450−459.
(57) Seo, M.; Kim, S. Y.; Kim, Y. D.; Park, E. D.; Uhm, S. Highly Stable Barium Zirconate Supported Nickel Oxide Catalyst for Dry Reforming of Methane: From Powders toward Shaped Catalysts. *Int. J. Hydrogen Energy* **2018**, *43* (24), 11355−11362.
(58) Balint, I.; You, Z.; Aika, K.-i. Morphology and Oxide Phase Control in the Microemulsion Mediated Synthesis of Barium Stabilized Alumina Nanoparticles. *Phys. Chem. Chem. Phys.* **2002**, *4* (12), 2501−2503.
(59) Liotta, L. F.; Deganello, G.; Sannino, D.; Gaudino, M. C.; Ciambelli, P.; Gialanella, S. Influence of Barium and Cerium Oxides on Alumina Supported Pd Catalysts for Hydrocarbon Combustion. *Appl. Catal. A Gen.* **2002**, *229* (1−2), 217−227.
(60) You, Z.; Inazu, K.; Balint, I.; Aika, K. I. Barium Hexaaluminate as a Novel Promising Support for Ruthenium-Based Ammonia Synthesis Catalysts. *Chem. Lett.* **2005**, *34* (5), 692−693.
(61) Gomes, R.; Costa, D.; Junior, R.; Santos, M.; Rodella, C.; Fréty, R.; Beretta, A.; Brandão, S. Dry Reforming of Methane over Nila-Based Catalysts: Influence of Synthesis Method and Ba Addition on Catalytic Properties and Stability. *Catalysts* **2019**, *9*, 313.
(62) Guo, M.; Lu, G. The Difference of Roles of Alkaline-Earth Metal Oxides on Silica-Supported Nickel Catalysts for CO_2 Methanation. *RSC Adv.* **2014**, *4* (102), 58171−58177.
(63) Yang, L.; Choi, Y.; Qin, W.; Chen, H.; Blinn, K.; Liu, M.; Liu, P.; Bai, J.; Tyson, T. A.; Liu, M. Promotion of Water-Mediated Carbon Removal by Nanostructured Barium Oxide/Nickel Interfaces in Solid Oxide Fuel Cells. *Nat. Commun.* **2011**, *2* (1), 357−359.
(64) Ersolmaz, C.; Falconer, J. L. Catalysed Carbon Gasif Ication with $Ba_{13}CO_3$. *Fuel.* **1986**, *65*, 400−406.
(65) Miyazaki, K.; Okanishi, T.; Muroyama, H.; Matsui, T.; Eguchi, K. Development of Ni−Ba(Zr,Y)O_3 Cermet Anodes for Direct Ammonia-Fueled Solid Oxide Fuel Cells. *J. Power Sources* **2017**, *365*, 148−154.
(66) Keller, M.; Matsuzaki, Y.; Otomo, J. CO_2 Activation by Methane in a Dual-Bed Configuration via Methane Cracking and Iron Oxide Lattice Oxygen Transport - Concept and Materials Development. *Chem. Eng. J.* **2018**, *349*, 249−259.
(67) Islam, S.; Hill, J. M. Barium Oxide Promoted Ni/YSZ Solid-Oxide Fuel Cells for Direct Utilization of Methane. *J. Mater. Chem. A* **2014**, *2* (6), 1922−1929.
(68) Zheng, M.; Wang, S.; Yang, Y.; Xia, C. Barium Carbonate as a Synergistic Catalyst for the H_2O/CO_2 Reduction Reaction at Ni-Yttria Stabilized Zirconia Cathodes for Solid Oxide Electrolysis Cells. *J. Mater. Chem. A* **2018**, *6* (6), 2721−2729.
(69) Niu, S.; Lv, W.; Zhou, G.; He, Y.; Li, B.; Yang, Q. H.; Kang, F. N and S Co-Doped Porous Carbon Spheres Prepared Using l-Cysteine as a Dual Functional Agent for High-Performance Lithium-Sulfur Batteries. *Chem. Commun.* **2015**, *51* (100), 17720−17723.
(70) Basahel, S. N.; Ali, T. T.; Mokhtar, M.; Narasimharao, K. Influence of Crystal Structure of Nanosized ZrO_2 on Photocatalytic Degradation of Methyl Orange. *Nanoscale Res. Lett.* **2015**, *10* (1), 73.
(71) Li, C.; Li, M. UV Raman Spectroscopic Study on the Phase Transformation of ZrO_2, Y_2O_3-ZrO_2 and $(SO_4)_2$-/ZrO_2. *J. Raman Spectrosc.* **2002**, *33* (5), 301−308.
(72) Rieder, K. H.; Weinstein, B. A.; Cardona, M.; Bilz, H. Measurement and Comparative Analysis of the Second-Order Raman Spectra of the Alkaline-Earth Oxides with a Nacl Structure. *Phys. Rev. B* **1973**, *8* (10), 4780−4786.
(73) Patel, R.; Fakeeha, A. H.; Kasim, S. O.; Sofiu, M. L.; Ibrahim, A. A.; Abasaeed, A. E.; Kumar, R.; Al-Fatesh, A. S. Optimizing Yttria-Zirconia Proportions in Ni Supported Catalyst System for H_2 Production through Dry Reforming of Methane. *Mol. Catal.* **2021**, *510* (April), 111676.
(74) Jia, X.; Zhang, X.; Rui, N.; Hu, X.; Liu, C.-j. Structural Effect of Ni/ZrO_2 Catalyst on CO_2 Methanation with Enhanced Activity. *Appl. Catal. B Environ.* **2019**, *244*, 159−169.
(75) Khatri, J.; Al-Fatesh, A. S.; Fakeeha, A. H.; Ibrahim, A. A.; Abasaeed, A. E.; Kasim, S. O.; Osman, A. I.; Patel, R.; Kumar, R. Ce Promoted Lanthana-Zirconia Supported Ni Catalyst System: A Ternary Redox System for Hydrogen Production. *Mol. Catal.* **2021**, *504*, 111498.
(76) Turcotte, R. P.; Sawyer, J. O.; Eyring, L. On the Rare Earth Dioxymonocarbonates and Their Decomposition. *Inorg. Chem.* **1969**, *8* (2), 238−246.
(77) Furniss, B. S.; Hannaford, A. J.; Smith, P. W. G.; Tatchell, A. R. *Vogel's Textbook of Practical Organic Chemistry*, 5th ed.; Longman Scientific & Technical: London, 1989; pp 1412−1422.
(78) Németh, M.; Srankó, D.; Károlyi, J.; Somodi, F.; Schay, Z.; Sáfrán, G.; Sajó, I.; Horváth, A. Na-Promoted Ni/ZrO_2 Dry Reforming Catalyst with High Efficiency: Details of Na_2O-ZrO_2-Ni Interaction Controlling Activity and Coke Formation. *Catal. Sci. Technol.* **2017**, *7* (22), 5386−5401.
(79) Bellido, J. D. A.; De Souza, J. E.; M'Peko, J. C.; Assaf, E. M. Effect of Adding CaO to ZrO_2 Support on Nickel Catalyst Activity in Dry Reforming of Methane. *Appl. Catal. A Gen.* **2009**, *358* (2), 215−223.
(80) Al-Fatesh, A. S.; Arafat, Y.; Kasim, S. O.; Ibrahim, A. A.; Abasaeed, A. E.; Fakeeha, A. H. In Situ Auto-Gasification of Coke Deposits over a Novel Ni-Ce/W-Zr Catalyst by Sequential Generation of Oxygen Vacancies for Remarkably Stable Syngas Production via CO2-Reforming of Methane. *Appl. Catal. B Environ.* **2021**, *280*, 119445.
(81) Al-Fatesh, A. S.; Arafat, Y.; Ibrahim, A. A.; Kasim, S. O.; Alharthi, A.; Fakeeha, A. H.; Abasaeed, A. E.; Bonura, G.; Frusteri, F. Catalytic Behaviour of Ce-Doped Ni Systems Supported on Stabilized Zirconia under Dry Reforming Conditions. *Catalysts* **2019**, *9* (5), 473.
(82) Tathod, A. P.; Hayek, N.; Shpasser, D.; Simakov, D. S. A.; Gazit, O. M. Mediating Interaction Strength between Nickel and Zirconia Using a Mixed Oxide Nanosheets Interlayer for Methane Dry Reforming. *Appl. Catal. B Environ.* **2019**, *249*, 106−115.
(83) García, V.; Fernández, J. J.; Ruíz, W.; Mondragón, F.; Moreno, A. Effect of MgO Addition on the Basicity of Ni/ZrO_2 and on Its Catalytic Activity in Carbon Dioxide Reforming of Methane. *Catal. Commun.* **2009**, *11* (4), 240−246.
(84) Xu, B. Q.; Wei, J. M.; Yu, Y. T.; Li, J. L.; Zhu, Q. M. Carbon Dioxide Reforming of Methane over Nanocomposite Ni/ZrO_2 Catalysts. *Top. Catal.* **2003**, *22* (1−2), 77−85.
(85) Li, X.; Chang, J.-S.; Tian, M.; Park, S.-E. CO2 Reforming of Methane over Modified Ni/ZrO_2 Catalysts. *Appl. Organomet. Chem.* **2001**, *15* (2), 109−112.
(86) Ibrahim, A. A.; Al-Fatesh, A. S.; Khan, W. U.; Kasim, S. O.; Abasaeed, A. E.; Fakeeha, A. H.; Bonura, G.; Frusteri, F. Enhanced Coke Suppression by Using Phosphate-Zirconia Supported Nickel Catalysts under Dry Methane Reforming Conditions. *Int. J. Hydrogen Energy* **2019**, *44* (51), 27784−27794.
(87) Kim, H.; Robertson, A. W.; Kwon, G. H.; Jang-Won, O.; Warner, J. H.; Kim, J. M. Biomass-Derived Nickel Phosphide Nanoparticles as a Robust Catalyst for Hydrogen Production by Catalytic Decomposition of C_2H_2 or Dry Reforming of CH_4. *ACS Appl. Energy Mater.* **2019**, *2* (12), 8649−8658.
(88) Nagaraja, B. M.; Bulushev, D. A.; Beloshapkin, S.; Ross, J. R. H. The Effect of Potassium on the Activity and Stability of Ni-MgO-ZrO_2 Catalysts for the Dry Reforming of Methane to Give Synthesis Gas. *Catal. Today* **2011**, *178* (1), 132−136.
(89) Fan, M. S.; Abdullah, A. Z.; Bhatia, S. Utilization of Greenhouse Gases through Carbon Dioxide Reforming of Methane over Ni-Co/MgO-ZrO_2: Preparation, Characterization and Activity. *Studies. Appl. Catal. B Environ.* **2010**, *100* (1−2), 365−377.
(90) Titus, J.; Roussière, T.; Wasserschaff, G.; Schunk, S.; Milanov, A.; Schwab, E.; Wagner, G.; Oeckler, O.; Gläser, R. Dry Reforming of Methane with Carbon Dioxide over NiO-MgO-ZrO_2. *Catal. Today* **2016**, *270*, 68−75.

https://doi.org/10.1021/acsomega.2c00471
ACS Omega 2022, 7, 16468−16483

(91) Chen, Q.; Zhang, J.; Pan, B.; Kong, W.; Chen, Y.; Zhang, W.; Sun, Y. Temperature-Dependent Anti-Coking Behaviors of Highly Stable Ni-CaO-ZrO_2 Nanocomposite Catalysts for CO_2 Reforming of Methane. *Chem. Eng. J.* **2017**, *320*, 63−73.
(92) Liu, S.; Guan, L.; Li, J.; Zhao, N.; Wei, W.; Sun, Y. CO_2 Reforming of CH_4 over Stabilized Mesoporous Ni-CaO-ZrO_2 Composites. *Fuel* **2008**, *87* (12), 2477−2481.
(93) Al-Fatesh, A. S.; Fakeeha, A. H.; Ibrahim, A. A.; Abasaeed, A. E. Ni Supported on La_2O_3+ZrO_2 for Dry Reforming of Methane: The Impact of Surface Adsorbed Oxygen Species. *Int. J. Hydrogen Energy* **2021**, *46* (5), 3780−3788.
(94) Al-Fatesh, A. S.; Khatri, J.; Kumar, R.; Kumar Srivastava, V.; Osman, A. I.; AlGarni, T. S.; Ibrahim, A. A.; Abasaeed, A. E.; Fakeeha, A. H.; Rooney, D. W. Role of Ca, Cr, Ga and Gd Promotor over Lanthana-Zirconia−Supported Ni Catalyst towards H_2-Rich Syngas Production through Dry Reforming of Methane. *Energy Sci. Eng.* **2022**, *10* (3), 866−880.
(95) Yao, L.; Galvez, M. E.; Hu, C.; Da Costa, P. Synthesis Gas Production via Dry Reforming of Methane over Manganese Promoted Nickel/Cerium-Zirconium Oxide Catalyst. *Ind. Eng. Chem. Res.* **2018**, *57* (49), 16645−16656.
(96) Kasim, S. O.; Al-Fatesh, A. S.; Ibrahim, A. A.; Kumar, R.; Abasaeed, A. E.; Fakeeha, A. H. Impact of Ce-Loading on Ni-Catalyst Supported over La_2O_3+ZrO_2 in Methane Reforming with CO_2. *Int. J. Hydrogen Energy* **2020**, *45* (58), 33343−33351.
(97) Kambolis, A.; Matralis, H.; Trovarelli, A.; Papadopoulou, C. Ni/CeO2-ZrO_2 Catalysts for the Dry Reforming of Methane. *Appl. Catal. A Gen.* **2010**, *377* (1−2), 16−26.
(98) Charisiou, N. D.; Siakavelas, G.; Tzounis, L.; Sebastian, V.; Monzon, A.; Baker, M. A.; Hinder, S. J.; Polychronopoulou, K.; Yentekakis, I. V.; Goula, M. A. An in Depth Investigation of Deactivation through Carbon Formation during the Biogas Dry Reforming Reaction for Ni Supported on Modified with CeO_2 and La_2O_3 Zirconia Catalysts. *Int. J. Hydrogen Energy* **2018**, *43* (41), 18955−18976.
(99) Baktash, E.; Littlewood, P.; Pfrommer, J.; Schomäcker, R.; Driess, M.; Thomas, A. Controlled Formation of Nickel Oxide Nanoparticles on Mesoporous Silica Using Molecular Ni_4O_4 Clusters as Precursors: Enhanced Catalytic Performance for Dry Reforming of Methane. *ChemCatChem.* **2015**, *7* (8), 1280−1284.
(100) Shi, L. Y.; Li, Y. X.; Xue, D. M.; Tan, P.; Jiang, Y.; Liu, X. Q.; Sun, L. B. Fabrication of Highly Dispersed Nickel in Nanoconfined Spaces of As-Made SBA-15 for Dry Reforming of Methane with Carbon Dioxide. *Chem. Eng. J.* **2020**, *390*, 124491.
(101) Zhang, J.; Li, F. Coke-Resistant Ni at SiO_2 Catalyst for Dry Reforming of Methane. *Appl. Catal. B Environ.* **2015**, *176−177*, 513−521.
(102) Gálvez, M. E.; Albarazi, A.; Da Costa, P. Enhanced Catalytic Stability through Non-Conventional Synthesis of Ni/SBA-15 for Methane Dry Reforming at Low Temperatures. *Appl. Catal. A Gen.* **2015**, *504*, 143−150.
(103) Huang, F.; Wang, R.; Yang, C.; Driss, H.; Chu, W.; Zhang, H. Catalytic Performances of Ni/Mesoporous SiO_2 Catalysts for Dry Reforming of Methane to Hydrogen. *J. Energy Chem.* **2016**, *25* (4), 709−719.
(104) Gao, X. Y.; Ashok, J.; Widjaja, S.; Hidajat, K.; Kawi, S. Ni/SiO_2 Catalyst Prepared via Ni-Aliphatic Amine Complexation for Dry Reforming of Methane: Effect of Carbon Chain Number and Amine Concentration. *Appl. Catal. A Gen.* **2015**, *503*, 34−42.
(105) Zhang, Q.; Tang, T.; Wang, J.; Sun, M.; Wang, H.; Sun, H.; Ning, P. Facile Template-Free Synthesis of Ni-SiO_2 Catalyst with Excellent Sintering- and Coking-Resistance for Dry Reforming of Methane. *Catal. Commun.* **2019**, *131*, 105782.
(106) Wang, C.; Jie, X.; Qiu, Y.; Zhao, Y.; Al-Megren, H. A.; Alshihri, S.; Edwards, P. P.; Xiao, T. The Importance of Inner Cavity Space within Ni@SiO_2 Nanocapsule Catalysts for Excellent Coking Resistance in the High-Space-Velocity Dry Reforming of Methane. *Appl. Catal. B Environ.* **2019**, *259*, 118019.
(107) Daoura, O.; Fornasieri, G.; Boutros, M.; El Hassan, N.; Beaunier, P.; Thomas, C.; Selmane, M.; Miche, A.; Sassoye, C.; Ersen, O.; Baaziz, W.; Massiani, P.; Bleuzen, A.; Launay, F. One-Pot Prepared Mesoporous Silica SBA-15-like Monoliths with Embedded Ni Particles as Selective and Stable Catalysts for Methane Dry Reforming. *Appl. Catal. B Environ.* **2021**, *280*, 119417.
(108) Quek, X. Y.; Liu, D.; Cheo, W. N. E.; Wang, H.; Chen, Y.; Yang, Y. Nickel-Grafted TUD-1 Mesoporous Catalysts for Carbon Dioxide Reforming of Methane. *Appl. Catal. B Environ.* **2010**, *95* (3−4), 374−382.
(109) Al-Fatesh, A. S.; Kumar, R.; Kasim, S. O.; Ibrahim, A. A.; Fakeeha, A. H.; Abasaeed, A. E.; Atia, H.; Armbruster, U.; Kreyenschulte, C.; Lund, H.; Bartling, S.; Ahmed Mohammed, Y.; Albaqmaa, Y. A.; Lanre, M. S.; Chaudhary, M. L.; Almubaddel, F.; Chowdhury, B. Effect of Cerium Promoters on an MCM-41-Supported Nickel Catalyst in Dry Reforming of Methane. *Ind. Eng. Chem. Res.* **2022**, *61*, 164.
(110) Tian, J.; Li, H.; Zeng, X.; Wang, Z.; Huang, J.; Zhao, C. Facile Immobilization of Ni Nanoparticles into Mesoporous MCM-41 Channels for Efficient Methane Dry Reforming. *Chin. J. Catal.* **2019**, *40* (9), 1395−1404.
(111) Hambali, H. U.; Jalil, A. A.; Abdulrasheed, A. A.; Siang, T. J.; Vo, D. V. N. Enhanced Dry Reforming of Methane over Mesostructured Fibrous Ni/MFI Zeolite: Influence of Preparation Methods. *J. Energy Inst.* **2020**, *93* (4), 1535−1543.
(112) Aguiar, M.; Cazula, B. B.; Saragiotto Colpini, L. M.; Borba, C. E.; Alves da Silva, F.; Noronha, F. B.; Alves, H. J. Si-MCM-41 Obtained from Different Sources of Silica and Its Application as Support for Nickel Catalysts Used in Dry Reforming of Methane. *Int. J. Hydrogen Energy* **2019**, *44* (60), 32003−32018.
(113) Li, W.; Zhao, Z.; Guo, X.; Wang, G. Employing a Nickel-Containing Supramolecular Framework as Ni Precursor for Synthesizing Robust Supported Ni Catalysts for Dry Reforming of Methane. *ChemCatChem.* **2016**, *8* (18), 2939−2952.
(114) Zhang, Q.; Zhang, T.; Shi, Y.; Zhao, B.; Wang, M.; Liu, Q.; Wang, J.; Long, K.; Duan, Y.; Ning, P. A Sintering and Carbon-Resistant Ni-SBA-15 Catalyst Prepared by Solid-State Grinding Method for Dry Reforming of Methane. *J. CO_2 Util.* **2017**, *17*, 10−19.
(115) Yang, W.; Liu, H.; Li, Y.; Wu, H.; He, D. CO_2 Reforming of Methane to Syngas over Highly-Stable Ni/SBA-15 Catalysts Prepared by P123-Assisted Method. *Int. J. Hydrogen Energy* **2016**, *41* (3), 1513−1523.
(116) Wang, M.; Zhang, Q.; Zhang, T.; Wang, Y.; Wang, J.; Long, K.; Song, Z.; Liu, X.; Ning, P. Facile One-Pot Synthesis of Highly Dispersed Ni Nanoparticles Embedded in HMS for Dry Reforming of Methane. *Chem. Eng. J.* **2017**, *313*, 1370−1381.
(117) Peng, H.; Zhang, X.; Han, X.; You, X.; Lin, S.; Chen, H.; Liu, W.; Wang, X.; Zhang, N.; Wang, Z.; Wu, P.; Zhu, H.; Dai, S. Catalysts in Coronas: A Surface Spatial Confinement Strategy for High-Performance Catalysts in Methane Dry Reforming. *ACS Catal.* **2019**, *9* (10), 9072−9080.
(118) Gao, X. Y.; Hidajat, K.; Kawi, S. Facile Synthesis of Ni/SiO_2 Catalyst by Sequential Hydrogen/Air Treatment: A Superior Anti-Coking Catalyst for Dry Reforming of Methane. *J. CO_2 Util.* **2016**, *15*, 146−153.
(119) Han, B.; Wang, F.; Zhang, L.; Wang, Y.; Fan, W.; Xu, L.; Yu, H.; Li, Z. Syngas Production from Methane Steam Reforming and Dry Reforming Reactions over Sintering-Resistant Ni@SiO_2 Catalyst. *Res. Chem. Intermed.* **2020**, *46* (3), 1735−1748.
(120) Chong, C. C.; Cheng, Y. W.; Bukhari, S. N.; Setiabudi, H. D.; Jalil, A. A. Methane Dry Reforming over Ni/Fibrous SBA-15 Catalysts: Effects of Support Morphology (Rod-Liked F-SBA-15 and Dendritic DFSBA-15). *Catal. Today* **2021**, *375*, 245−257.
(121) Xu, Y.; Lin, Q.; Liu, B.; Jiang, F.; Xu, Y.; Liu, X. A Facile Fabrication of Supported Ni/Sio2 Catalysts for Dry Reforming of Methane with Remarkably Enhanced Catalytic Performance. *Catalysts* **2019**, *9* (2), 183.
(122) Li, Z.; Jiang, B.; Wang, Z.; Kawi, S. High Carbon Resistant Ni@Ni Phyllosilicate@SiO_2 Core Shell Hollow Sphere Catalysts for

https://doi.org/10.1021/acsomega.2c00471
ACS Omega 2022, 7, 16468−16483

Low Temperature CH_4 Dry Reforming. *J. CO_2 Util.* **2018**, *27*, 238−246.
(123) Xie, T.; Shi, L.; Zhang, J.; Zhang, D. Immobilizing Ni Nanoparticles to Mesoporous Silica with Size and Location Control via a Polyol-Assisted Route for Coking- and Sintering-Resistant Dry Reforming of Methane. *Chem. Commun.* **2014**, *50* (55), 7250−7253.
(124) Kang, D.; Lim, H. S.; Lee, J. W. Enhanced Catalytic Activity of Methane Dry Reforming by the Confinement of Ni Nanoparticles into Mesoporous Silica. *Int. J. Hydrogen Energy* **2017**, *42* (16), 11270−11282.
(125) Zhang, Q.; Sun, M.; Ning, P.; Long, K.; Wang, J.; Tang, T.; Fan, J.; Sun, H.; Yin, L.; Lin, Q. Effect of Thermal Induction Temperature on Re-Dispersion Behavior of Ni Nanoparticles over Ni/SBA-15 for Dry Reforming of Methane. *Appl. Surf. Sci.* **2019**, *469*, 368−377.
(126) Chong, C. C.; Setiabudi, H. D.; Jalil, A. A. Dendritic Fibrous SBA-15 Supported Nickel (Ni/DFSBA-15): A Sustainable Catalyst for Hydrogen Production. *Int. J. Hydrogen Energy* **2020**, *45* (36), 18533−18548.
(127) Mourhly, A.; Kacimi, M.; Halim, M.; Arsalane, S. New Low Cost Mesoporous Silica (MSN) as a Promising Support of Ni-Catalysts for High-Hydrogen Generation via Dry Reforming of Methane (DRM). *Int. J. Hydrogen Energy* **2020**, *45* (20), 11449−11459.
(128) Pan, C.; Guo, Z.; Dai, H.; Ren, R.; Chu, W. Anti-Sintering Mesoporous Ni−Pd Bimetallic Catalysts for Hydrogen Production via Dry Reforming of Methane. *Int. J. Hydrogen Energy* **2020**, *45* (32), 16133−16143.
(129) Abd Ghani, N. A.; Azapour, A.; Syed Muhammad, A. F. ad; Abdullah, B. Dry Reforming of Methane for Hydrogen Production over Ni-Co Catalysts: Effect of Nb-Zr Promoters. *Int. J. Hydrogen Energy* **2019**, *44*, 20881−20888.
(130) Ibrahim, A. A.; Fakeeha, A. H.; Al-Fatesh, A. S. Enhancing Hydrogen Production by Dry Reforming Process with Strontium Promoter. *Int. J. Hydrogen Energy* **2014**, *39* (4), 1680−1687.
(131) Vroulias, D.; Gkoulemani, N.; Papadopoulou, C.; Matralis, H. W−Modified Ni/Al_2O_3 Catalysts for the Dry Reforming of Methane: Effect of W Loading. *Catal. Today* **2020**, *355*, 704−715.
(132) Abasaeed, A.; Kasim, S.; Khan, W.; Sofiu, M.; Ibrahim, A.; Fakeeha, A.; Al-Fatesh, A. Hydrogen Yield from CO_2 Reforming of Methane: Impact of La_2O_3 Doping on Supported Ni Catalysts. *Energies* **2021**, *14*, 2412.
(133) Hu, X.; Jia, X.; Zhang, X.; Liu, Y.; Liu, C.-j. Improvement in the Activity of Ni/ZrO_2 by Cold Plasma Decomposition for Dry Reforming of Methane. *Catal. Commun.* **2019**, *128*, 105720.

https://doi.org/10.1021/acsomega.2c00471
ACS Omega 2022, 7, 16468−16483